Spacecraft Interplanetary Navigation Using Radiometric Tracking and Accelerometer Measurements

Sandro Papais

Bachelor of Engineering

Mechanical Engineering Department

McGill University

Montreal, Quebec

April 2018

A thesis submitted to McGill University in partial fulfillment of the requirements of the Undergraduate Honours Program

ABSTRACT

There is a continued and increasing interest in deep-space missions in order to study planetary bodies and asteroids in the solar system. In order to estimate the position of a spacecraft traversing the solar system, radiometric tracking using the Deep Space Network (DSN) is primarily used. Currently, Gedex Systems Inc. is developing a new-technology measurement device called the Vector Gravimeter/Accelerometer (VEGA) that will be able to measure acceleration with unprecedented accuracy. VEGA has the potential to enable inertial navigation for low-thrust applications, such as deep-space missions, which have previously not been possible due to large measurement errors. This study investigates how VEGA can be used with radiometric tracking measurements for a low-thrust interplanetary spacecraft mission. A model of a spacecraft traversing the solar system is developed. Using VEGA for dead-reckoning of position and DSN measurements for position correction, a study of how frequently DSN measurements are needed to correct the dead-reckoning solution provided by VEGA is undertaken. The study found that the use of VEGA for dead-reckoning will allow a threefold increase in the amount of time needed between radio tracking sessions. Over the duration of a mission to the main asteroid belt, VEGA would allow for over one million USD in reduced mission operation costs associated with tracking. These results would allow a spacecraft to reduce its dependence on the DSN, thus also enabling the DSN to manage a larger number concurrent interplanetary missions.

ABRÉGÉ

Il existe un intérêt continu et grandissant envers les missions d'exploration spatiales, dans le but d'étudier les corps planétaires et astéroïdes du système solaire. Afin d'estimer la position d'un engin spatial à travers le système solaire, la localisation radiométrique du réseau de communications avec l'espace lointain (DSN) est la méthode la plus utilisée. Présentement, Gedex Systems Inc. développe un nouvel appareil de mesure appelé le Gravimètre/Accéléromètre Vectoriel (VEGA), capable de mesurer l'accélération avec un degré de précision inégalé. Le VEGA a le potentiel de permettre la navigation inertielle pour les applications de faible poussée, telles que les missions dans l'espace lointain, auparavant rendues impossible par l'amplitude des erreurs de mesure. Cette étude explore la manière dont le VEGA peut être utilisé, couplé avec des données de localisation radiométrique, pour une sonde interplanétaire à faible poussée. Un modèle de l'engin spatial traversant le système solaire a été développé. En utilisant le VEGA comme outil de navigation, ainsi que les mesures du DSN pour corriger la dérive inertielle, l'étude de la fréquence des mesures nécessaires à la correction de la solution à l'estime du VEGA a été entreprise. L'étude a montré que l'utilisation du VEGA pour le guidage permet de tripler les intervalles nécessaires entre les séquences de suivi radio. Sur la durée d'une mission jusqu'à la ceinture d'astéroïdes principale, ceci permet de réduire les frais d'exploitation associés à la localisation de plus d'un million USD. Ces résultats permettent donc aux engins spatiaux de diminuer leur dépendance au DSN, et ainsi permettre au DSN de servir un plus grand nombre de missions interplanétaires.

ACKNOWLEDGEMENTS

First and foremost, I would like to express my gratitude to my supervisor and mentor, Professor James Forbes. I am grateful for the opportunity to work and start my research career with him. His continued support and guidance have made my time with his research group a very memorable and enriching experience. I would also like to thank Dr. Kieran Carroll for providing a very interesting and rewarding research topic. I could always count on him sharing his advice and extensive knowledge with me throughout the research process. Finally, I would like to thank my parents for allowing me to follow my passion and for their continued support.

TABLE OF CONTENTS

LIST OF TABLES

LIST OF FIGURES

CHAPTER 1
Introduction

Interplanetary spacecraft navigation is the process of determining the state of a spacecraft at a given time in order to predict and correct the trajectory for desired mission objectives. The navigation process typically involves acquisition of radiometric tracking signals from Earth and optical measurements on-board the spacecraft. These observations are used to form a best estimate of the position and velocity of the vehicle. The spacecraft's state information is then used to verify performance and plan maneuvers to target points of interest on distant bodies. Several trends in planetary science and exploration are placing increasingly stringent requirements and constraints on navigation technology which will need to be met in order to enable the next generation of interplanetary missions.

1.1 Background

Interplanetary navigation has been an active field of research since the early 1960s when interplanetary robotic exploration first began. In order to facilitate these missions into deep space, typically defined as those operating at or beyond the orbit of the Earth's Moon, a network of ground tracking and communications facilities were developed. All deep-space missions require some form of ground-station tracking and telecommunications network to transmit data to and from the spacecraft. There are several ground stations used for deep space tracking operations, including sites operated by the space agencies of the USA, Europe, Russia, Japan, India, and China. The NASA JPL Deep Space Network (DSN), is one of the largest and most sophisticated of these networks, it was also the first, established in 1958 [1]. It has facilities located in Goldstone, California; Madrid, Spain; and Canberra, Australia. As shown in Figure 1–1, these locations are chosen to be approximately 120 degrees of longitude apart to ensure continual coverage for tracking of deep space vehicles.

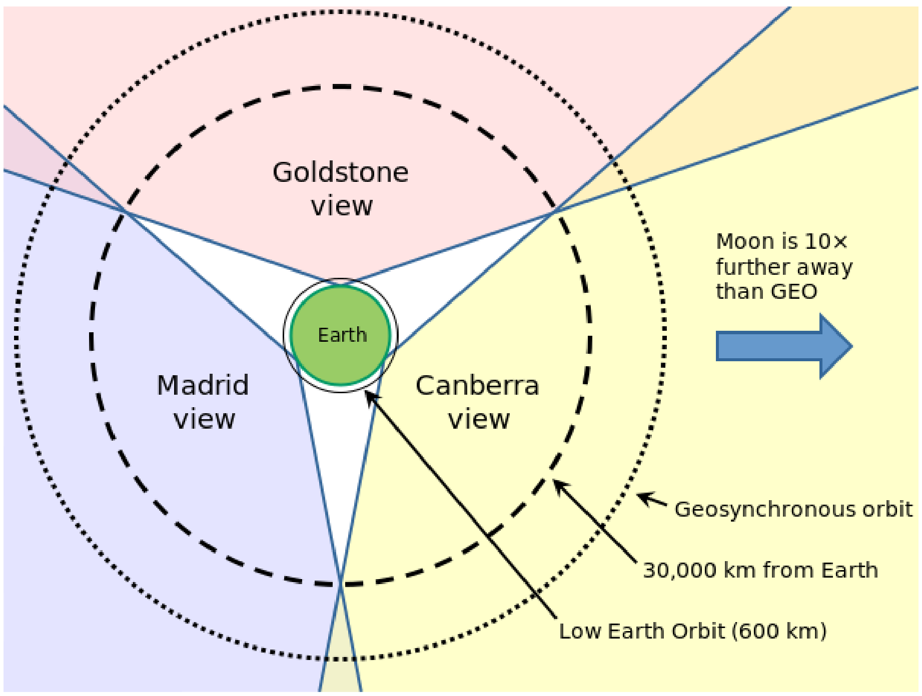

Figure 1–1: DSN tracking facilities field of view, as viewed from Earth's north pole.

The DSN was designed to communicate with spacecraft traveling between a distance of 16,000km from Earth to the furthest planets in the solar system [2]. Once a mission reaches a distance of more than 30,000 km from earth, it will always be in view of at least one of the stations. At specific intervals each day the spacecraft can also be tracked by two stations enabling differential radiometric techniques, which compares signals at two different stations to infer information about the spacecraft's trajectory. The capabilities of the DSN have dramatically improved over the years. When it was first established it had a downlink rate of 10^{-3} bits/s at 5 AU using S-Band tracking. As of 2017 capabilities using Ka-band have reached as high at 10^8 bits/s, equivalent to that needed for an HDTV [3]. Similarly, the accuracy of tracking measurements have increased drastically since the first interplanetary mission in 1962.

While the DSN's navigation capabilities have increased drastically in six decades of spaceflight, it is not currently able to achieve many of the upcoming missions proposed in the next decade. The Guidance, Navigation, and Control (GN&C) Technology Assessment for Future Planetary Science Missions [4] study performed by NASA JPL in 2012 found that in order to meet many objectives of the next generation of deep space missions, spacecraft need be able to achieve one meter navigational accuracy in the vicinity of small bodies and tens of meters planetary landing accuracy in the near term. In comparison, recent mission capabilities have an accuracy an order of magnitude lower than this. Continued advancements will be necessary in order to enable the success of more complex missions such as multi-body planetary tours, planetary landing, in proximity operations around small bodies, and touch-and-go contact with low-gravity objects, sample capture, and sample return.

There are several challenges associated with interplanetary navigation that must be taken into consideration in order meet navigational requirements. Vast distances, on the order of millions of kilometers, much be traveled by spacecraft in order to reach precise locations on bodies of interest in the solar system. These targets are also constantly moving in relatively well known orbits around other bodies. The study of the motion of man-made objects in space, subject to both natural and artificially induced forces is known as astrodynamics. Highly accurate astrodynamics modeling can be very challenging due to uncertainties in ephemeris (positions of naturally occurring astronomical objects) and non-gravitational disturbing forces. Additional constraints on hardware performance limits are imposed due to the particularly harsh conditions of space causing large temperature variations and intense radiation experienced by the spacecraft. Size and weight constraints are also imposed due to the challenges and high costs associated with escaping Earth's gravity and atmosphere. Mission duration is also an important factor. Since most interplanetary missions span several years, hardware reliability is essential to operate effectively in these harsh conditions over time with minimal degradation. The large distances traveled by the spacecraft also complicates communication with operators on Earth. Any radio signals sent from a spacecraft can experience hours of round trip light-time delay in reaching Earth.

A key consideration in interplanetary mission design is the choice of propulsion system and trajectory design. Spacecraft propulsion can be broadly classified into three types: chemical combustion rockets, electric propulsion, and non-internal reacting mass systems. Combustion spacecraft engines were the first flight proven propulsion system and are currently the most common. Electric propulsion systems followed; the first demonstration in space was in 1964 by NASA's SERT-1 (Space Electric Rocket Test) and subsequently first flight proven by the Soviet Union's Zond

2 in the same year for attitude control applications. Non-internal reacting mass systems, most notably as solar sails, have also been gaining interest lately. The first true solar sail voyage was made by JAXA in 2010 and several flight demonstrations are being scheduled in the near future.

Most interplanetary missions have used combustion propulsion, with near impulsive maneuvers lasting only minutes, to achieve the delta-v (change in velocity) required. In contrast, electric propulsion produces significantly less thrust, on the order of mN, but can operate over the majority of the mission duration. Electric thrusters use much less propellant compared to chemical combustion systems since they have higher exhaust speed which is to say they operate at a higher specific impulse. Current advanced electric propulsion design are anticipated to be able to impart a delta-v of over 100km/s throughout the mission, compared to the typical high-end delta-v produced on current chemical systems of 7km/s [5]. This will be increasingly useful to execute missions to more distant, outer planets in our solar system in a timely manner.

The use of electric propulsion in interplanetary missions has been steadily increasing over the last 20 years, this trend is expected to continue as reliability and cost reductions continue to grow. It is anticipated that the entire spacecraft market will reach 50% electric propulsion adoption by 2020.

1.2 Motivation

The methods of interplanetary navigation have not changed significantly over time, relying mainly on several radiometric methods and on-board optical measurements. These technologies have been used to varying degrees in interplanetary missions and have benefited from ever-increasing precision and accuracy. However, due to increasingly stringent mission requirements for future planetary science investigations, there is a growing demands for higher accuracy and autonomous response of spacecraft to new environments. Current missions use a ground-processing paradigm where ground stations must receive data, process it, and send it back to spacecraft. As is discussed in [6], this paradigm causes the timeliest trajectory solutions available on-board for typical distances (to Mar's and beyond) to be stale by half an hour or more as a result of lighttime delays and ground station processing time, making it unable to meet many future mission requirements.

The importance of navigation in enabling future exploration is also emphasized in the technology evaluation done by The Nation Academy of Sciences in 2012 titled "NASA Space Technologies and Roadmaps and Priorities; Restoring NASA's Technological Edge and Paving the Way for a New Era in Space" [7]. This assessment places GN&C technology in the top priority list for two of the three NASA Objective areas. For the Objective B, "Explore the evolution of the solar system and the potential for life elsewhere, GN&C is categorized as the top priority for NASA. Within navigation, the top technical challenge and highest priority technology are considered to be accurate onboard autonomous navigation and maneuvering systems. These will be critical for future missions to meet necessary capabilities increases and reduced ground support requirements. A higher degree of onboard autonomy will reduce dependence for routine position fixes from earth which will free networks for other tasks. The alignment of this technology to all deep space mission needs is also very high since it will impact all types of exploration including science missions, robotic explorers, planetary landers, and crewed missions.

In the broader space industry several relevant emerging trends will also have an effect on navigation requirements. Spacecraft are becoming more capable, reliable, compact, and less costly due to emerging technologies. In addition, the cost of access to space has fallen due to commercial launch vehicle development and reusablility efforts. This is expected to further increase volume of interplanetary missions and increase awareness of the need for lower costs per interplanetary mission. This trend can be seen in the general nano-satellite market which has grown substantially over recent years, with expectations to continue as shown in figure 1–2. A similar trend can also be seen in the continued and increasing interest in deep-space missions in order to study planetary bodies or asteroids.

In general, using deep space ground facilities for radiometric tracking is extremely resource intensive and costly for the users. For example, in 2007 dollars the cost of using the DSN range from 954 USD per hour of contact for the 34 meter antenna to 4770 USD per hour of contact for use of a 70 meter antenna, not including charges for an additional hour for setup and shutdown costs [8]. Assuming weekly tracking sessions which is currently typical, this accumulates to tens of thousands of dollars per week and millions of USD per year.

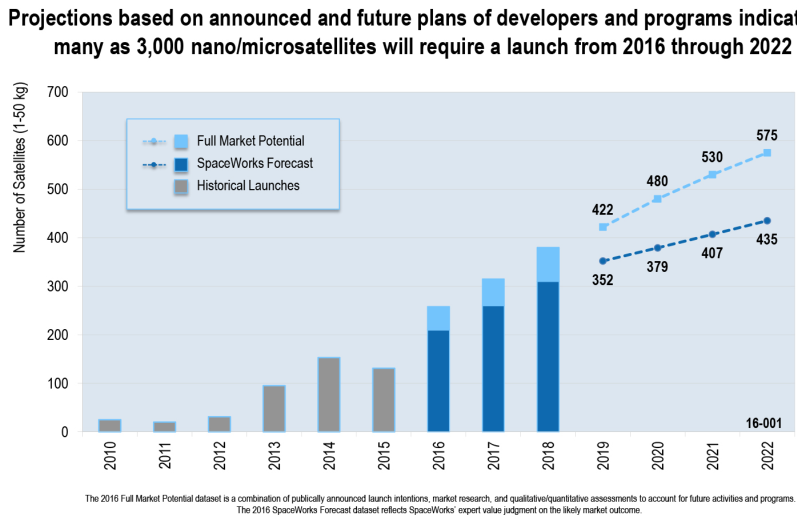

Figure 1–2: Nano-satellite market forecast. Growth in the satellite market is expected to continue, creating challenges for communication and tracking stations.

As the number of concurrent deep-space missions grows, there is a need to reduce reliance on deep space tracking facilities, such as the DSN. The finite capacity of these networks is likely to be a large constraint on the development of future deep space missions. Due to the high costs for tracking and the growing number of concurrent deep-space missions there is a need to reduce reliance on deep space tracking facilities. This will be facilitated by increased autonomy and on-board navigation.

Additional technologies that will be crucial for future deep space missions are solar power generation and electric propulsion. Due to the long duration of interplanetary missions, often lasting several years, solar electric propulsion systems offer several advantages. Electric propulsion has been shown to be significantly safer and more efficient than chemical ones. Solar power generation has been crucial to all past exploration missions and has vital complementary importance for meeting higher power requirements of electric propulsion. This combination requires much less on-board propellant compared to conventional chemical combustion propulsion to produce the same effective delta-v over a longer duration. This leads to spacecraft mass savings resulting in reduced launch costs and increased specific force during flight. Electric propulsion also offers the ability for deeper throttleability ranges making it possible to control the spacecraft's position more accurately. Solar and electric propulsion technologies are also set as the second and third top priorities, after GN&C, for space exploration set out by the NRC as shown in table 1–1.

Table 1–1: NASA top technology priorities, categorized by objective [7].

Extend and sustain human activities beyond low Earth orbit	Explore the evolution of the solar system and the potential for life elsewhere (in situ measurements)	Expand understanding of the Earth and the universe (remote measurements)
Radiation Mitigation for Human Spaceflight	**GN&C**	Optical Systems (Instruments and Sensors)
Long-Duration Crew Health	**Solar Power Generation (Photovoltaic and Thermal)**	High-Contrast Imaging and Spectroscopy Technologies
ECLSS	**Electric Propulsion**	Detectors and Focal Planes
GN&C	Fission Power Generation	Lightweight and Multifunctional Materials and Structures
(Nuclear) Thermal Propulsion	EDL TPS	Active Thermal Control of Cryogenic Systems
Lightweight and Multifunctional Materials and Structures	In Situ Instruments and Sensors	**Electric Propulsion**
Fission Power Generation	Lightweight and Multifunctional Materials and Structures	**Solar Power Generation (Photovoltaic and Thermal)**
EDL TPS	Extreme Terrain Mobility	

Solar electric propulsion (SEP) creates additional challenges to interplanetary navigation. Gravitational forces for all the main bodies in the Solar system are by now extremely well known and can be modeled to a high degree of precision; however, effects due to the variability of thrust over long periods can have major effects on trajectory. As experienced on the Deep Space 1 mission, ion propulsion has instances of thrust cut-off when power supplies are turned off momentarily to clear faults [9]. There is also a dependency of the propulsion system on its power source, which is relative to the efficiency of solar panels and solar radiation received. Both of these factors are subject to change as solar panels degrade, as the spacecraft's distance varies relative to the sun, and due to solar cycles or variations. Even with extremely frequent tracking sessions, the Deep Space 1 operators realized precise predictions to the target were impossible due to the unplanned thrust changes that invariably occurred as discussed in [9]. It is clear that SEP navigation will experience significant uncertainties in the predictability of expected thrust and possible degradation of thruster performance and power sources.

In order to enable onboard navigation these variations in SEP must be determined and accounted for. A promising approach to doing so is accelerometers onboard to measure acceleration produced in real-time. With current accelerometer technology, use of accelerometer measurements for low-thrust spacecraft navigation has not been possible due to relatively large measurement errors compared to spacecraft accelerations. However, a new generation of nano-G accelerometers show promise for enabling this solution. For example, Gedex Systems Inc. is developing a new-technology measurement device called the Vector Gravimeter/Accelerometer (VEGA) that will be able to measure acceleration with unprecedented accuracy. VEGA functions as a three-axis absolute (zero bias) accelerometer, with potential for enabling the first application of inertial navigation methods to spacecraft equipped with low-thrust propulsion systems. The prototype for VEGA shown in figure 1–3 has already been ground tested as a proof of concept.

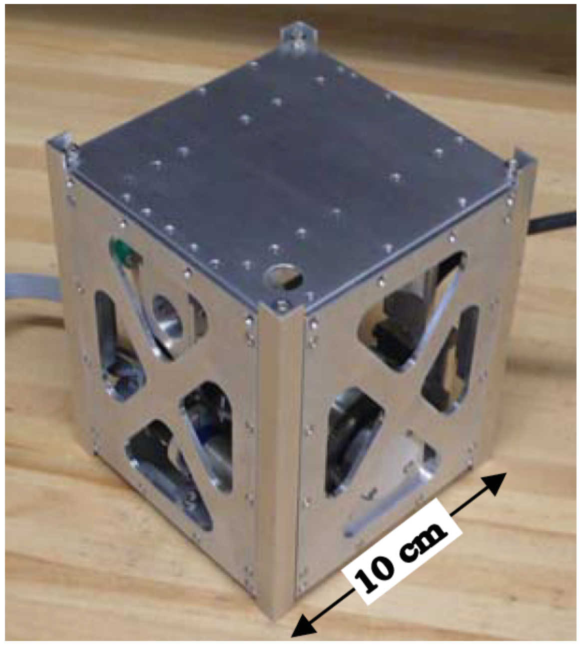

Figure 1–3: VEGA mechanical breadboard prototype.

Many missions scenarios, including low-thrust navigation, requiring GN&C are currently dominated by IMU errors. VEGA may have the accuracy to alter the execution of these missions from necessitating continuous navigation updates, through radiometric and optical measurements, to those that can rely on dead-reckoning for extended periods of time. Using a previously determined position fix, dead-reckoning would use accelerometer measurements to advance and update the spacecraft's position over time with limited errors. The ability to perform low-thrust dead-reckoning would ultimately enable on-board autonomous low-thrust navigation. In addition to dead-reckoning applications, major reasons for inertial navigation in low-thrust missions include early detection of malfunctions or large off-nominal performance changes (as previously experienced) and to better characterize performance variations of low-thrust propulsion systems in space.

Nano-G accelerometers like VEGA are also included as highest priority navigation technologies with potential to dramatically improve planetary atmospheric aerobraking, crewed mission, touch and go (TAG) missions, and planetary entry, descent, and landing (EDL) [6], [10]. In fact, several proposed next generation missions have significant technology dependence on future nano-G accelerometers. These missions include Mars sample return entry phase, comet surface sample return, lunar south pole-Aitken Basin sample return, trojan asteroid tour and rendezvous, NEO surveyor explorer, planetary defense precursor, and microNEO explorer [10].

1.3 Research Objectives

The focus of the remainder of this manuscript will be on low-thrust interplanetary navigation using radiometric tracking and VEGA accelerometer measurements. The conjecture upon which this work is based on is that a low-thrust propulsion system will produce a force vector different from what is expected, causing the predicted spacecraft position and velocity to become increasingly different from the actual spacecraft state. As discussed previously in Section 1.2 this has been in the case in previous demonstration missions and can be reasonably expected in future missions.

The primary objective of this work is to evaluate how accurately VEGA inertial navigation can be used to estimate an actual trajectory over time, for a spacecraft that is undergoing low-acceleration thrusting and whose magnitude and direction are uncertain relative to what is being commanded. The goal of the analysis is to establish the inertial navigation dead-reckoning accuracy versus time, through modeling VEGA's performance characteristics in a low-thrust mission. The trajectory will be propagated assuming dead-reckoning using VEGA measured thrust and this will be compare to the actual trajectory. The analysis will be carried out for a range of reasonable uncertainties using a Monte-Carlo simulation. Finally, VEGA's limits in the navigation process will be quantified along with the impact on extending mission capabilities and reducing mission costs.

1.4 Thesis Outline

In Chapter 2 a review of the current state of the art for interplanetary navigation is performed. An overview of the current navigation processes and performance will be undertaken. Emphasis is placed on radiometric tracking and inertial navigation methods. The issues with the current low-thrust navigation paradigm will also be discussed.

Chapter 3 will provide a mathematical framework to analyze VEGA's dead reckoning performance. First, the relevant reference frames will be defined. Next, three equations of motion will be derived to compare VEGA's performance to current methods of navigation. Stochastic methods will be used to simulate the random variations experienced during the low-thrust trajectory. Finally, a method for interplanetary trajectory targeting will be shown.

In chapter 4, several validation cases will be shown to verify the models performance. Visualization of the trajectory and conservation of energy principles will be used in the case of no thrust. For constant thrust change in energy will be compared with work performed by thrust.

Chapter 5 will present the results from the preliminary off-nominal effects study. It will also discuss the results of the Monte Carlo simulation to assess VEGA's dead reckoning capability. These results will be applied to a mission scenario to show the impact of the results.

Finally, Chapter 6 will summarize the work done and the significance. It will also propose future investigation needed to build on this study.

CHAPTER 2
Literature Review

2.1 Interplanetary Navigation Processes

The typical deep space navigation process can be broken into three main functions; observations, orbit determination, and guidance. The observation measurement systems includes antennas for radar and optical sensors for attitude orientation and target relative position measurements. The orbit determination process estimates the flight path using the observed measurements, predictive models of the spacecraft's trajectory, and expected process noise. Guidance is then used to propagate the last known state of the spacecraft, as estimated by orbit determination, to the target. Guidance will then determine how the nominal mission burns will be achieved. If a large difference exists between the predicted and desired future state a trajectory correction maneuver (TCM) is needed and the subsystem will compute the required delta-V maneuverer.

These subsystems interact with each other continuously throughout the mission. The navigation process can be visualized in the context of a feedback control system as shown in figure 2–1, with the desired spacecraft trajectory being the system input and the actual trajectory as the output. The general deep space navigation process is summarized in [11] along with capabilities of navigation in 1975.

In order to create high fidelity simulations of the spacecraft, the dynamics of the system must be well understood and modeled. Significant work has been done in

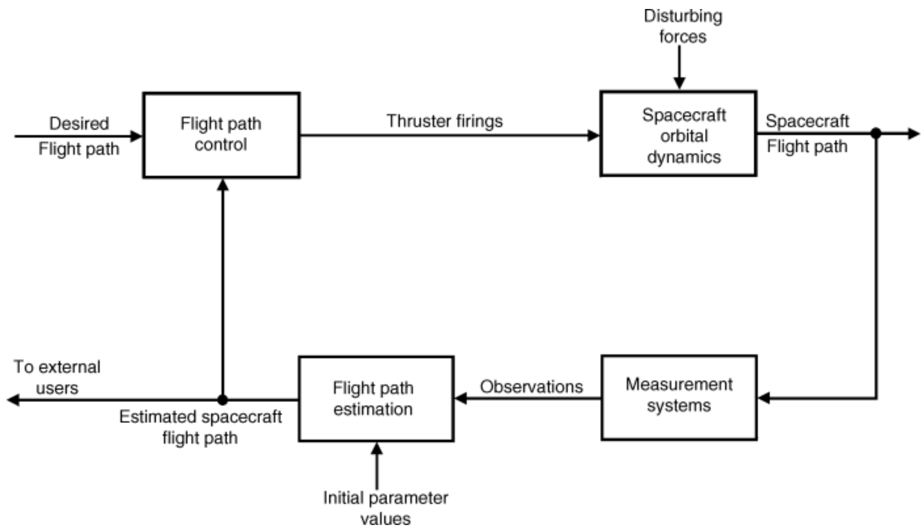

Figure 2–1: Simplified deep space navigation system block diagram. Here orbit determination and guidance systems are referred to as flight path estimation and flight path control respectively.

summarizing the key concepts of astrodynamics, most comprehensively by Vallado [12] and Bate et al. [13]. Key topics include equations of motion such as Kepler's Laws (two-body motion) and Newton's Laws (generalized N-body motion), orbital elements state representation, coordinate systems, observations, orbital maneuvering, perturbation techniques, orbit determination, estimation, and optimization.

Optimization, also referred to as optimal control, is a general concept that can be implemented in various subjects such as economics and chemistry, but is particularly useful for trajectory design. Early optimal control applications were developed by Bryson and Ho in 1975 [14]. The method of adjoining the terminal constraint to the cost functions using Lagrange multiplier, also known as the adjoint method, was introduced in their book. Based on this method, a particular problem about optimizing the duration of time of transferring a satellite from low Earth orbit to geostationary orbit was discussed. More recent treatments of the optimization problem can also be found in [15], [16], and [17].

Orbit determination is an iterative procedure of estimating a spacecraft's trajectory based on spacecraft dynamics and observation models. These models produce predicted observations which are compared to the actual observation measurements taken. The difference between the two data sets, known as residuals, should exhibit purely random or Gaussian distribution due to uncorrelated errors. If there are errors in the trajectory model it will be noticeable and model parameters are adjusted, often through weighted linear least squares estimation. The process of covariance analysis effects due to mismodeled variables and incorrect filter a priori statistics is further described in [18].

Orbit determination processing typically uses a batch-sequential least-squares or Kalman filter to determine the best estimate of the state of the spacecraft and adjust model parameters to minimize residual errors [11]. In most onboard applications in the aerospace fields, typically a Kalman filter formulation is used which continuously updates the filter information. However, historically in deep space navigation missions speed has not been as critical and often there was a lack of reliable data points available onboard [19]. This was the case in past autonomous demonstration missions such as Deep Space 1 which used radiometric and onboard optical measurements along with a batch filtering approach for navigation.

Once the model of the trajectory is known to be reliable, the guidance system is used to determine the optimal trajectory or correction maneuver if necessary. This navigation process, shown in figure 2–2, is carried out at specific intervals, typically weekly, over the course of a mission. Accuracy requirements for residuals can vary drastically depending on the objective.

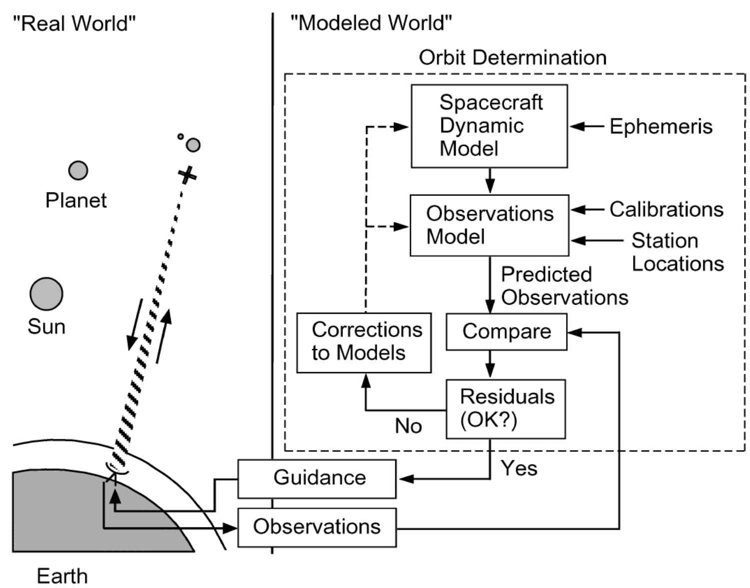

Figure 2–2: The navigation process. Observations are made and compared to predictions which are iteratively corrected through orbit determination. Once the estimated trajectory has sufficient convergence the guidance system calculates the optimal maneuvers and commands to execute them [20].

In order to achieve required navigation constraints optical navigation instruments have been used extensively along side radiometric tracking during interplanetary missions. Typically there is some uncertainty in the position of the target body which requires a method for inferring precise target relative position. Originally, this was resolved through radiometric tracking sessions once the spacecraft is close enough to the target for its gravitational field to affect its trajectory measurably. Subsequently, optical navigation methods were developed using camera imaging. Several images are taken of a nearby body over time against a background of distant stars. The images are then processed to determine where the spacecraft is relative to the body. These images are typically sent back to ground stations for processing but efforts have been made to process onboard for autonomous navigation, such as described for the Deep Space 1 mission in [21]. Other common optical sensors include star trackers and sun sensors which used extensively in spacecraft attitude determination and control.

2.2 Interplanetary Mission Performance

The first successful planetary flyby mission was achieved by NASA's Mariner 2 spacecraft, launched in 1962 to Venus. As described in [22] single mid-course maneuver was performed to compensate for orbit injection errors, achieving a targeting flyby error of 15,000 km. The spacecraft system design, shown in figure 2–3, was used as the foundation that several interplanetary missions to follow built upon. The navigation relevant hardware used at this time was limited to sun sensors, attitude control gas bottles, and a high-gain directional antenna. By the time of the first successful flight to Mars by NASA's Mariner 4 in 1965 it was possible to reach a target delivery accuracy on the order of a thousand kilometers. A decade later the NASA Viking 1 mission was launched to Mars and by this time the accuracy of interplanetary navigation has improved further by a factor of 100. This enabled a targeting accuracy on the order of tens of kilometers for the terrestrial planets (Mercury, Venus and Mars) and hundreds of kilometers for Jupiter and Saturn [23]. This improvement in part enabled the NASA's Mariner 10 spacecraft to become the first to visit Mercury and the first to use another planet (Mercury) as a gravity assist.

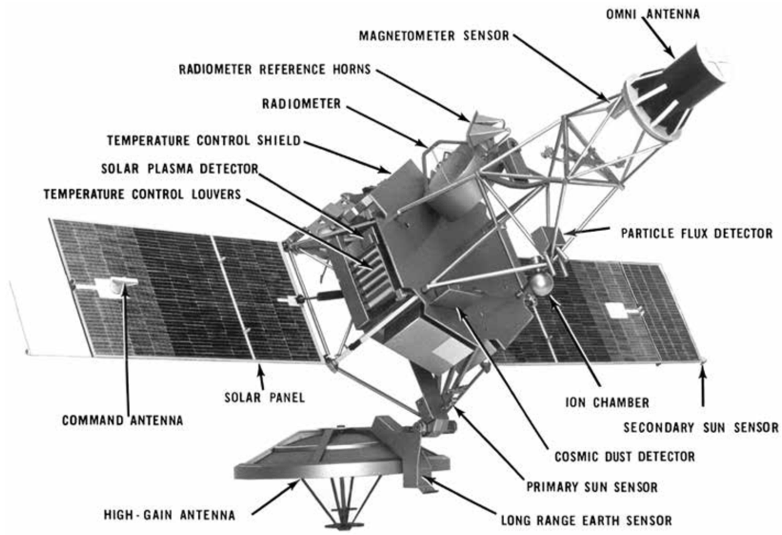

Figure 2–3: System design of NASA JPL's Mariner 2, the first successful interplanetary spacecraft.

This general trend continued, along with increasing mission requirements and performance criteria. In 2001, the NASA Mars Odessey mission using daily radar tracking sessions, was able to achieve a periphrasis altitude error of 0.7km with four TCM on the journey [24]. In 2003, the Mars Explorer Rovers (MER) used six TCM to land on Mars with impact distance errors of only 180 m and 750 m for MER-A and MER-B respectively. By 2005, accuracy to distant bodies such as asteroids and comets was achieved within a few kilometer of flyby accuracy using radiometric and optical methods by the NASA Stardust (2004), ESA Rosetta (2004), NASA Deep Impact (2005) missions [25]. From the first successful planetary mission in 1962 to modern missions four decades later, this represented a six order of magnitude decrease in navigation targeting error. As discussed in [22] these improvements were largely due to increases in computing capabilities and techniques, allowing more sophisticated modeling. The addition of on-board imaging systems substantially improved target-relative navigational accuracy, reducing the impact of target body ephemeris uncertainties. The development of differential range measurements across two tracking stations contributed to substantially reduce angular uncertainty.

The first interplanetary spacecraft to use electric propulsion and low-thrust navigation was NASA's Deep Space 1 (DS1) mission with an ion propulsion system (IPS), launched in 1998. It was a demonstration mission part of the New Millennium Program, dedicated to testing advanced technologies. The primary goal of DS1 was to successfully test and validate 12 technologies. A flyby of asteroid 19992KD (Braille) was scheduled in July 1999 as a "science bonus" and the mission was eventually extended to comet Borrelly in September 2001. The DS1 primary mission was analyzed and discuss in detail in [9]. The primary mission trajectory was broken into two main mission burns with a requirement of two and a half months thrusting with the IPS during the nine months between launch and encounter. After initial check out, the thrusting profile was broken into roughly one week segments. Each thrust segment was followed by optical image acquisition and radiometric tracking with the IPS switched off for necessary attitude control. Radiometric tracking was limited to range and Doppler with a 10 hour high gain antenna (HGA) tracking pass, often using pass offs between stations for differential range information.

The navigation of DS1 assumed position uncertainty of 150km based on 1 percent thrust magnitude and 10 μrad thrust direction. One-week prediction had errors of well over 450km, mostly due to predictable thrust-level changes [9]. In order to perform initial system check out and long term performance verification IPS acceptance tests (IAT) 1 and 2 were scheduled at the beginning and near the end of primary mission respectively. IAT2 came after nearly 1800 hours of IPS thrusting, and tested several different nominal thrust magnitudes. IAT2 showed a thrust uncertainty of 0.04 mN in magnitude and 0.12 deg and 1 degree uncertainty for in-plane and normal thrust directions. IAT2 also showed a 1.1 to 1.5 percent decrease from IAT1 and 1.29 to 2.05 decrease from nominal expected thrust. Thrust magnitude variations can be seen in figure 2–4 and compared in table 2–1 to nominal and IAT1 performance.

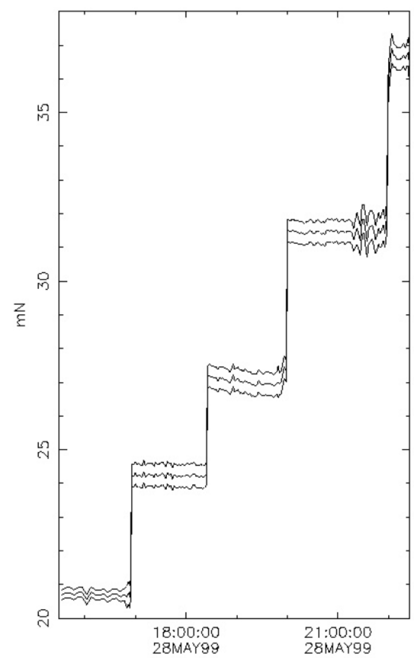

Figure 2–4: DS1 IAT2 IPS thrust performance estimate with 1-σ error corridor.

Table 2–1: DS1 IPS thrust performance estimate.

Nominal Thrust, mN (thrust level index)	IPS1 thrust, mN (percent from nominal)	IAT2 thrust, mN (percent from nominal)
20.7 (#6)	20.797 ± 0.125 (+0.49 ± 0.60)	20.705 ± 0.082 (+0.05 ± 0.40)
24.6 (#13)		24.234 ± 0.065 (-1.29 ± 0.26)
27.5 (#20)		26.985 ± 0.073 (-1.75 ± 0.27)
32.1 (#2)	31.766 ± 0.214 (-1.10 ± 0.67)	31.460 ± 0.074 (-2.05 ± 0.23)
37.4 (#34)		36.616 ± 0.231 (-1.98 ± 0.62)
47.9 (#48)	47.298 ± 0.140 (-1.19 ± 0.29)	
63.2 (#69)	62.227 ± 0.412 (-1.49 ± 0.65)	
73.6 (#83)	72.561 ± 0.408 (-1.41 ± 0.55)	
78.4 (#90)	77.388 ± 0.449 (-1.27 ± 0.57)	

Low thrust navigation was also demonstrated in ESA's Small Missions for Advanced Research in Technology 1 (SMART-1) and JAXA's Hayabusa in 2003. SMART-1 used a solar-powered Hall effect thruster to reach and orbit Earth's moon. Hayabusa was the first sample return mission to an asteroid which also used ion propulsion. The subsequent use of ion propulsion was in the first NASA's exploration mission Dawn in 2007. This allowed Dawn to accumulate enough delta-V needed to enter and leave orbit of multiple celestial bodies, whereas previous multi-target missions using conventional combustion drives were restricted to flybys [26]. Similar to DS1, Dawn also had weekly thrusting sessions broken up with coast phases for tracking, as shown in figure 5–17.

More recently JAXA's PROCYON mission, the first micro-satellite (50 kg) deep space exploration satellite, showed the feasibility of electric propulsion on a low cost (a few million dollars) and one year development project [27]. Also, the NASA high powered (12.5 kW) electric propulsion concept known as the Hall Effect Rocket

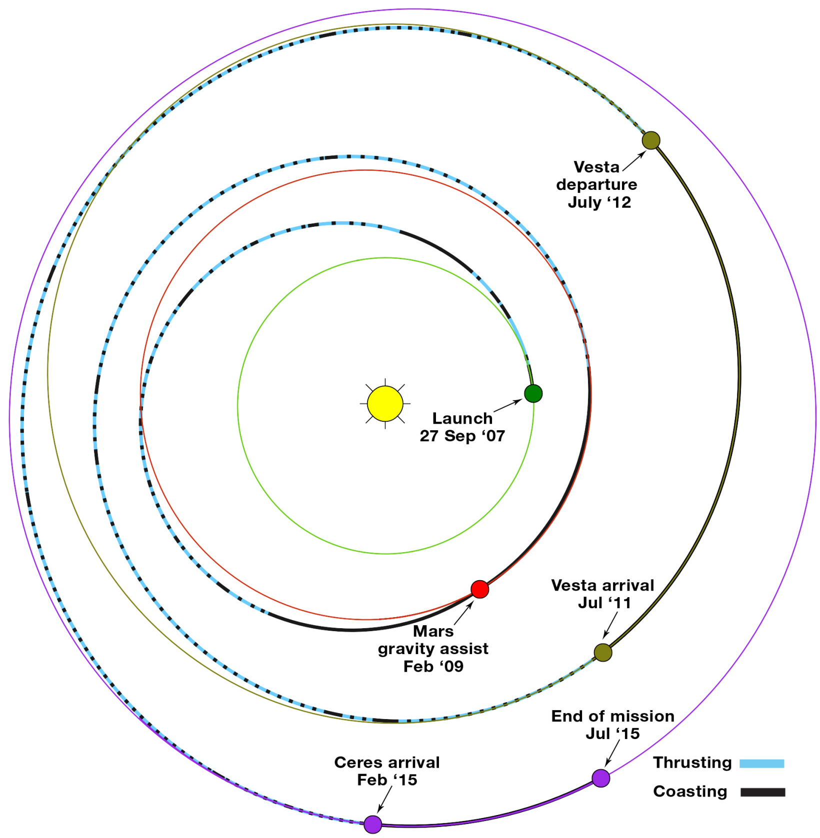

Figure 2–5: Trajectory overview for Dawn mission, showing thrust and coast segments.

with Magnetic Shielding (HERMeS), which would be the largest electric propulsion system yet, had ground demonstration characterization in 2016 [28].

2.3 Radiometric Tracking

Several navigational tracking measurements have been developed to achieve the objective of interplanetary navigation. The current methods involve two-way Doppler, two-way ranging, and delta differential one-way range (delta-DOR) using the spacecraft's X-band communications system. Typical accuracies for these DSN metric observables are 0.06 mm/sec for line-of-sight velocity, 75 cm for line-of-sight distance, and 2.5 nrad for angular position [29].

Tracking spacecraft in deep space, is done most frequently through radio link between the spacecraft and Earth. The first measurement developed was Doppler tracking. This method measures the frequency shift of electromagnetic radiation caused by the relative motion of the spacecraft resolved in the direction of the line of sight, known as range rate. In order to measure the range rate, the frequency of the source must be known precisely before the shift. The received frequency is

$$f_{rec} = f + \frac{fv}{c}, \tag{2.1}$$

where f is the spacecraft's source frequency, v is the spacecraft's velocity, and c is the speed of light. However, a spacecraft's transmitter has many limitations which prevent it from outputting a stable precise frequency. In order to solve this a method called coherence is used. Since DSN complexes are able to provide very stable frequencies, they are supplied in uplink to the spacecraft which generates a downlink back which is phase-coherent. This is referred to as two-way coherent mode which generates extremely high accuracy Doppler measurements. The current error standard deviation for Xband Doppler data with a oneminute count time is typically about 0.06mm/s [29].

Beyond line of sight relative velocity of the spacecraft, it is also possible to measure the line of sight distance from the tracking station known as range. Ranging uses a radio uplink from the DSN carrying a recognizable signal called ranging tones. These are sent back to the DSN ranging system which records the timing of the

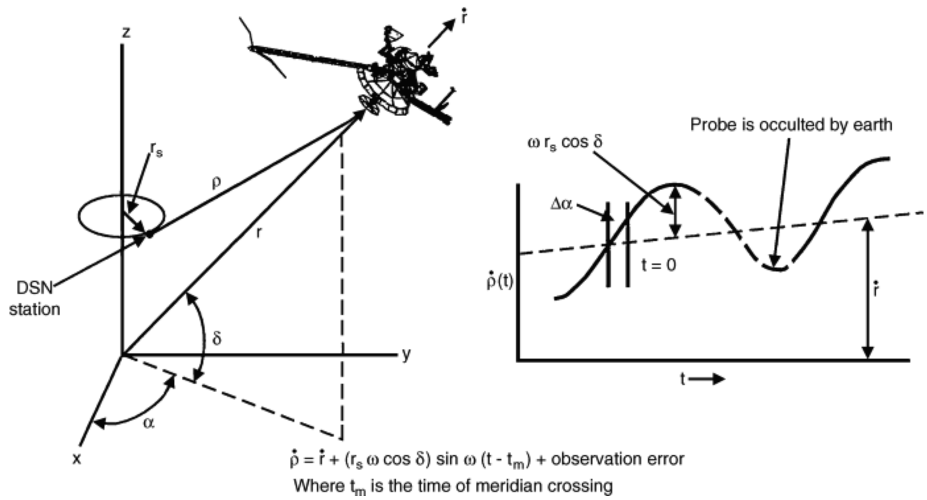

Figure 2–6: Doppler measurement process. In addition to determining line of sight velocity, angular information can be obtained through diurnal effects.

ranging tones uplink and downlink. The elapsed time gives the distance traveled by the signal traveled at the speed of light, this distance being the range data. This requires very accurate timekeeping, on the sub-nanosecond scale, at the DSN ground station to achieve range measurements to a fraction of a meter. Several factors must be accounted for achieve the required time keeping, including the delay caused by electronics within the spacecraft, distance between DSN antenna to receivers to computers, relativistic effect, correction for speed through different media and atmospheric effects [30]. Error standard deviation for Xband range is currently approximately 0.75m, including both random and systematic effects [29].

Ranging and Doppler over time can be used to determine angular position of the spacecraft in terms of right ascension. However, measuring the declination, that is the north-south dimension in the plane-of-sky, can be particularly challenging and limited in its accuracy. In particular, the inaccuracy is extremely susceptible to small mismodelled forces. One such problems contribute to the loss of the Mars Climate Orbiter in 1999 where a trajectory error was made which accumulated in the declination direction which were not resolved or identified [31]. To address this a third radiometric method was developed in the for use in deep space, called very long baseline interferometry (VLBI).

VLBI technology uses broadband microwave radiation emitted by radio sources such as satellites and extragalactic quasars. By measuring these signals across two widely separated tracking stations, separated by a baseline, the signals can be analyzes to determine the difference in arrival time. This differential time of arrival, known as the VLBI delay or differential one-way range (DOR), can be expressed as

$$\tau_g = \frac{1}{c}\vec{B} \cdot \hat{s}, \tag{2.2}$$

where $\vec{B}$ is the baseline vector between the two stations, $\hat{s}$ is the unit vector to the target, and c is the speed of light. Therefore, all that is needed to determine the target direction is accurate prior knowledge of the baseline and measurement of the VLBI delay. From this it is apparent that the accuracy of this measurement system is dependent on the calibration of station clock off-sets, instrument delays, and baseline errors. In order to minimize these uncalibrated errors a second distant target with well known position, typically an extragalactic quasars, is used in a method known as delta differential one-way range (delta-DOR).

Based on the information provided by Thorton and Border (2000) [20], performance of DSN ΔVLBI observations are quite accurate. Typical accuracy of the system in 1992 was 16 nrad. while the error budget is dependent highly on geometry,

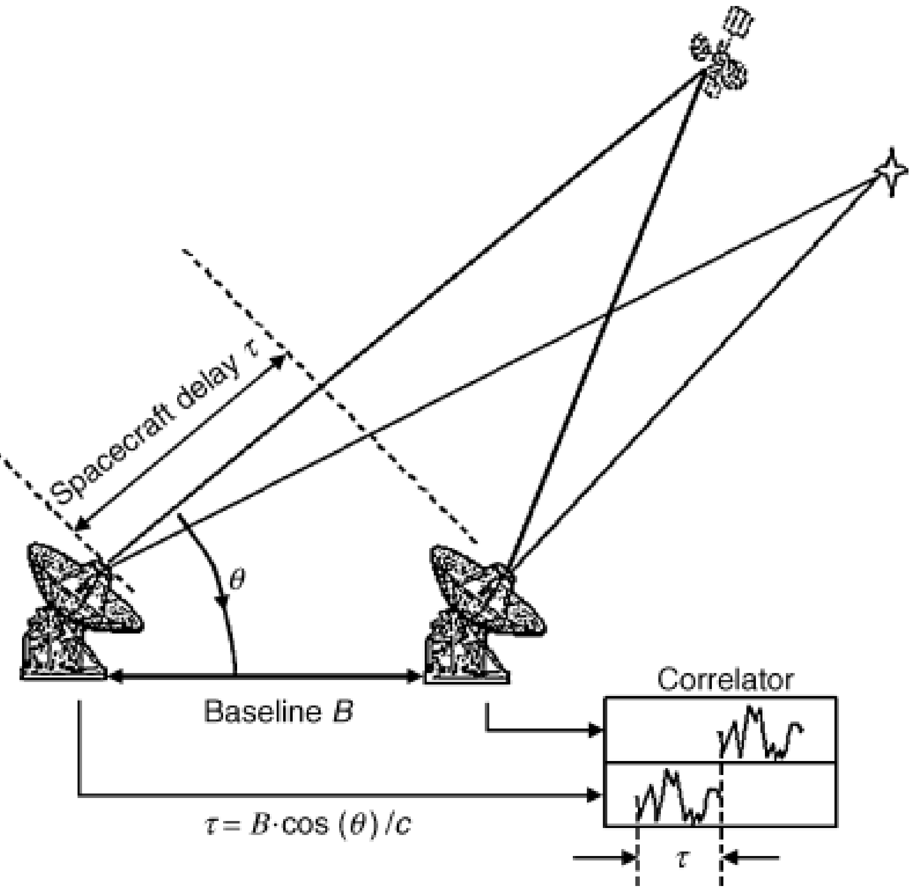

Figure 2–7: VLBI measurement correlation process.

even in the most unfavorable geometry, with the spacecraft lying in the ecliptic plane and large angular separation with the quasar, a measurement accuracy of 50 nrad was possible. This was later improved by the next generation tracking system in 2008, offering typical errors of 2.5 nrad [29]. The major sources of error in present day ΔDOR observations are typically measurement signal-to-noise ratios (SNRs), uncalibrated troposphere delays, baseline errors, and instrumental delays, shown in Figure 2–8.

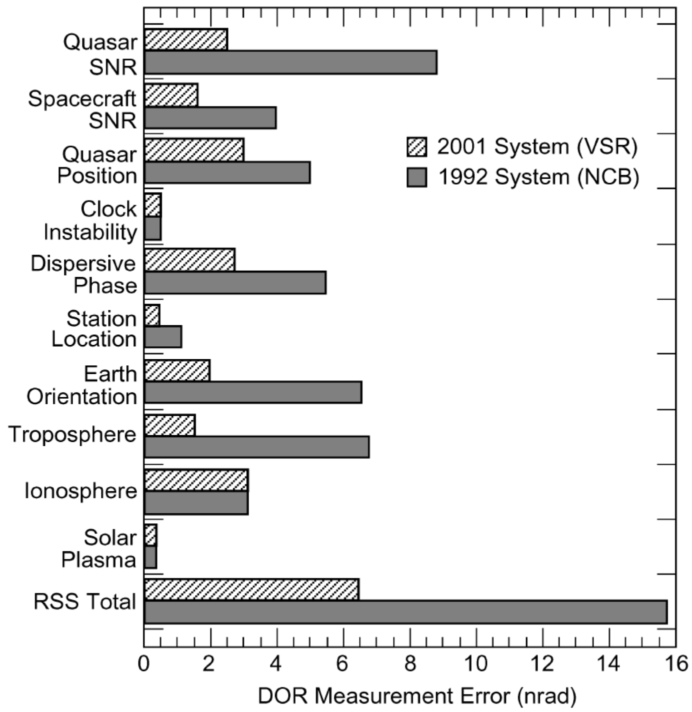

Figure 2–8: Error budget for VLBI measurement systems for both first and second generation tracking systems [20].

While VLBI is capable of determining angular position in plane of sky very accurately, it is resource intensive. Since the signals measured are typically very weak there is a need for very large antennas and low-noise receivers. Two stations must have antenna apertures of at least 34-m to both be available during limited windows of opportunity [20]. As a result, several effort have been made more recently for on-board navigation.

2.4 Inertial Navigation

The principles of modern inertial guidance first emerged in the 1940's during World War II in the Vl and V2 rockets by German engineers. This followed by significant developments for seaborne and airborne applications in the 1950's and standard military adoption in the 1960's in aircrafts, ballistic missiles, ships, and submarines. Several categories of inertial sensor technology have made significant progress in the last two decades. Development of micro-machined electromechanical systems (MEMS) devices has several advancements that are enabling new applications and improved performance.

Inertial navigation typically involves measurement of specific force (inertial acceleration plus gravity), removal of computed gravitation by feedback, double integration of indicated acceleration, and keeping track of orientation through attitude or angular rate sensors [32]. There are two main categories of inertial measurement units (IMUs), stable platform and strapdown systems, which are based on the frame of reference in which the rate-gyroscopes and accelerometers operate. Stable platform systems have inertial sensors mounted on a platform which is held in a constant orientation, using a feedback control system that is driven by an attitude estimate produced by the inertial navigation system. In a strapdown system, the inertial sensors are mounted rigidly onto the platform, therefore making measurements directly in the body frame rather than the global frame. In this case the rate gyroscope measurements are integrated to keep track of orientation. Benefits of strapdown systems are reduced mechanical complexity and smaller size. Drawbacks include increased computational complexity; however, as the cost of computation has decreased strapdown systems have become the dominant type of IMU [33].

The two main sensors used are typically angular rate sensors and translational accelerometers. A gyroscope measures angular velocity and there are several types, including mechanical, optical, and MEMS gyroscope. Linear accelerometers are used to measure specific force in three axis and can be classified as mechanical, solid state, and MEMS. Several error types can affect the performance of both of these sensors. Constant bias can cause steadily growing angular error and quadratically growing position error, white noise will cause random walk of the angle and position, and temperature effects and calibration will cause orientation and position drift errors [33].

Modern high performance accelerometers now are able to reach performance measurements with an accuracy on the order of nano-g. Accuracy varies with local gravity/acceleration field strength. It can be estimated that VEGA's absolute accuracy of 110 nanoG (110 Gal) is anticipated on a small asteroid. On the Moon, absolute accuracy of 0.11 G (0.11 mGal) is expected.

CHAPTER 3
Mathematical Model

In this chapter, the governing equations of motion, observational frames of reference, and uncertainty of measurements will be outlined. First, the two-dimensional Newtonian Mechanics Equations will be presented, followed by a summary of the coordinate systems and measurements. Finally, uncertainty will be modeled in the form of noise and used to evaluate VEGA's performance.

3.1 Reference Frames

The first step for performing spacecraft dynamic analysis is to define the reference frames and the geometry of motion. In order to describe the motion of a spacecraft in deep space we will begin by defining three commonly used coordinate systems.

The first frame is the geocentric equatorial frame, $\mathcal{F}_g$, also know as the Earth-centered inertial (ECI) frame. $\boldsymbol{\mathcal{F}}_g = [\underset{\rightarrow}{g}^1 \; \underset{\rightarrow}{g}^2 \; \underset{\rightarrow}{g}^3]^\intercal$, where $\underset{\rightarrow}{g}^2$ points towards the vernal equinox, $\underset{\rightarrow}{g}^3$ points towards the Earth's north pole, and $\underset{\rightarrow}{g}^1 = \underset{\rightarrow}{g}^2 \times \underset{\rightarrow}{g}^3$. Therefore $\boldsymbol{\mathcal{F}}_g$ has its fundamental plane in the Earth's equator and does not rotate with diurnal rotation of the earth.

The spacecraft state can be described using 6-parameter state vector of position and velocity components. In $\mathcal{F}_g$ the state vector is defined as $\boldsymbol{x}_g = [x_{g1} \; x_{g2} \; x_{g3} \; \dot{x_{g1}} \; \dot{x_{g2}} \; \dot{x_{g3}}]^\intercal$. However it is often more conveniently defined as $[r \; \alpha \; \delta \; \dot{r} \; \dot{\alpha} \; \dot{\delta}]^\intercal$, where r is the the earth center relative distance known as range, α is the angle of right ascension, δ is the angle of declination. $\dot{r}$, $\dot{\alpha}$, and $\dot{\delta}$ are the time derivatives of the range (known as range rate), right ascension, and declination respectively. $\boldsymbol{\mathcal{F}}_g$ along with the state parameters are shown in figure 3–1. Deep space tracking facilities will observe r, α, and δ directly through radiometric tracking, therefore these parameters will be used to simulate tracking measurements.

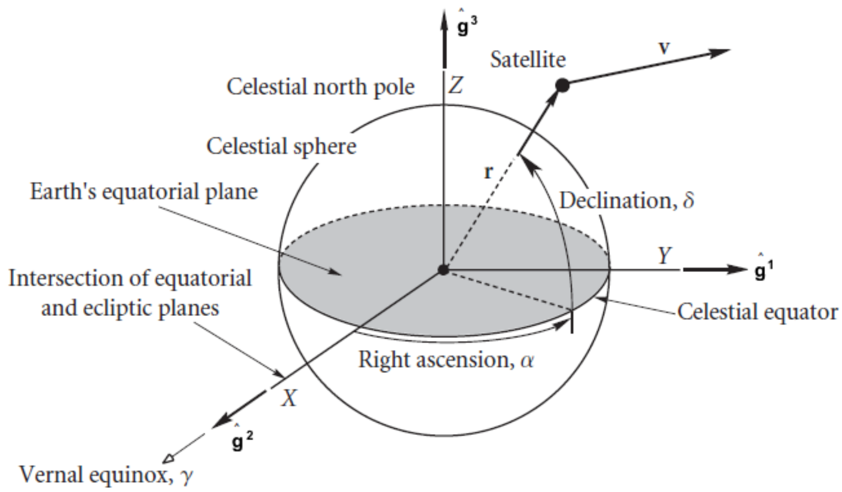

Figure 3–1: The geocentric equatorial frame, the standard earth based coordinate system. The position of a spacecraft relative to earth is commonly described using range, right ascension, declination.

$\mathcal{F}_g$ is the coordinate system that Earth based measurement's will be made in. However, modeling of interplanetary trajectories is most conveniently performed in heliocentric ecliptic frame $\mathcal{F}_h$. The frame is defined as $\boldsymbol{\mathcal{F}}_h = [\underrightarrow{h}^1\ \underrightarrow{h}^2\ \underrightarrow{h}^3]^\mathsf{T}$, where $\underrightarrow{h}^1$ points towards the winter solstice, $\underrightarrow{h}^2$ points towards the vernal equinox, and $\underrightarrow{h}^3 = \underrightarrow{h}^1 \times \underrightarrow{h}^2$. The state vector used in $\mathcal{F}_h$ represents the Cartesian coordinates of the spacecraft. Namely, $\boldsymbol{x}_h = [x_{h1}\ x_{h2}\ x_{h3}\ \dot{x_{h1}}\ \dot{x_{h2}}\ \dot{x_{h3}}]^\mathsf{T}$.

Since modeling of the interplanetary trajectory will be performed in $\mathcal{F}_h$, it will be necessary to later convert the state to $\mathcal{F}_g$ for analysis of Earth-based measurements. The state in heliocentric frame can be transformed to the ECI frame using a counterclockwise rotation of 23.44^o, the angle between the celestial and ecliptic north pole, in the $\underrightarrow{h}^2$ direction as shown in figure 3–2.

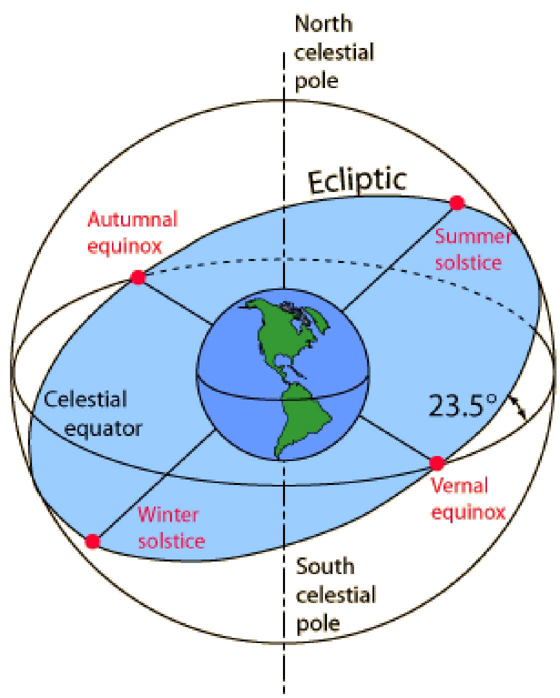

Figure 3–2: The heliocentric ecliptic frame, $\mathcal{F}_h$, shown with respect to the geocentric equatorial frame, $\mathcal{F}_g$. $\mathcal{F}_h$ can be related to the $\mathcal{F}_g$ by a rotation along the vernal equinox.

The third reference frame is the spacecraft body frame $\mathcal{F}_b$. This frame rotates with the spacecraft as it travels along its trajectory. The frame is defined as $\boldsymbol{\mathcal{F}}_b = [\underrightarrow{b}^1\ \underrightarrow{b}^2\ \underrightarrow{h}^3]^\mathsf{T}$, where $\underrightarrow{b}^2$ points in the direction of the velocity vector, $\underrightarrow{b}^3 = \underrightarrow{h}^3$, and $\underrightarrow{b}^1 = \underrightarrow{b}^2 \times \underrightarrow{b}^3$. The state vector used in $\mathcal{F}_b$ is $\boldsymbol{x}_b = [x_{b1}\ x_{b2}\ x_{b3}\ \dot{x_{b1}}\ \dot{x_{b2}}\ \dot{x_{b3}}]^\mathsf{T}$.

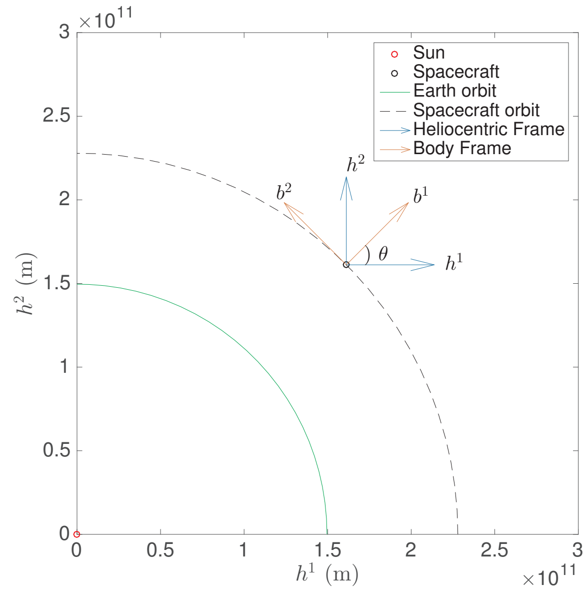

Figure 3–3: The heliocentric equatorial frame and spacecraft body frame shown for a spacecraft in a counterclockwise circular heliocentric orbit near Mars.

3.2 Nominal Trajectory Equations of Motion

In order to develop the dynamics of the spacecraft we start with Newton's second law for a two body gravitational system using Cowell's Method. Here the spacecraft will be referred to as the vehicle for purposes of notation. Consider force on the vehicle due to gravity

$$\underset{\rightarrow}{f}^{vg} = \frac{G m_s m_v \underset{\rightarrow}{r}^{vs}}{\left\| \underset{\rightarrow}{r}^{vs} \right\|^3}, \tag{3.1}$$

where G is the universal gravitational constant, m_s is the mass of the Sun, m_v is the mass of the vehicle or spacecraft, and $\underset{\rightarrow}{r}^{vs}$ is position of the vehicle relative to the Sun.

When resolved in $\mathcal{F}_h$, (3.1) becomes

$$\underset{\rightarrow}{f}^{vg} = \boldsymbol{\mathcal{F}}_h^{\mathsf{T}} \frac{Gm_s m_v(\mathbf{r}_h^{vb} - \mathbf{r}_h^{sb})}{\left\|\mathbf{r}_h^{vb} - \mathbf{r}_h^{sb}\right\|^3}, \tag{3.2}$$

where $\mathbf{r}_h^{vb}$ and $\mathbf{r}_h^{sb}$ are the positions of the vehicle and Sun relative to point b respectively. Point b is the barycenter of the system. Since point b will be very close to the position of the Sun, $\mathbf{r}_h^{sb}$ is assumed to be negligible and $\mathbf{r}_h^{vb} = \mathbf{r}_h^{vs}$, therefore (3.2) can be further simplified to

$$\underset{\rightarrow}{f}^{vg} = \boldsymbol{\mathcal{F}}_h^{\mathsf{T}} \frac{Gm_s m_v \mathbf{r}_h^{vs}}{\|\mathbf{r}_h^{vs}\|^3}.$$

The force on the vehicle due to the nominal thrust of the propulsion system is

$$\underset{\rightarrow}{\bar{f}}^{vt} = \frac{T \underset{\rightarrow}{v}^{vs}}{\left\|\underset{\rightarrow}{v}^{vs}\right\|}, \tag{3.3}$$

where T is the nominal magnitude of thrust produced by the vehicle and $\underset{\rightarrow}{v}^{vs}$ is the velocity of the vehicle with respect to the Sun. When resolved in $\mathcal{F}_h$, (3.3) becomes

$$\underset{\rightarrow}{\bar{f}}^{vt} = \boldsymbol{\mathcal{F}}_h^{\mathsf{T}} \frac{T\mathbf{v}_h^{vs}}{\|\mathbf{v}_h^{vs}\|}. \tag{3.4}$$

The acceleration of the vehicle due to combined effects of gravity and thrust, relative to the the Sun with respect to $\mathcal{F}_h$ is

$$\underset{\rightarrow}{a}^{vs/h} = \underset{\rightarrow}{v}^{vs/h^{\bullet h}} = \frac{\underset{\rightarrow}{f}^{vg} + \underset{\rightarrow}{\bar{f}}^{vt}}{m_v} = \frac{\mu_s \underset{\rightarrow}{r}^{vs}}{\left\|\underset{\rightarrow}{r}^{vs}\right\|^3} + \frac{T \underset{\rightarrow}{v}^{vs}}{m_v \left\|\underset{\rightarrow}{v}^{vs}\right\|}, \tag{3.5}$$

where $\mu_s = Gm_s$. When resolved in $\mathcal{F}_h$, (3.5) becomes

$$\underset{\rightarrow}{a}^{vs/h} = \underset{\rightarrow}{\boldsymbol{\mathcal{F}}}_h^{\mathsf{T}} \left(\frac{\mu_s \mathbf{r}_h^{vs}}{\|\mathbf{r}_h^{vs}\|^3} + \frac{T\mathbf{v}_h^{vs}}{\|\mathbf{v}_h^{vs}\|} \right). \tag{3.6}$$

Finally, (3.6) is used as the nominal acceleration of the vehicle and is numerically solved using the Runge-Kutta method in MATLAB.

3.3 Truth Trajectory Equations of Motion

In order to simulate the actual mission trajectory, the nominal equation of motion will be perturbed with noise similar to that experienced in mission due to acceleration fluctuations. The truth equation of motion is given by the acceleration of the vehicle with respect to the sun relative to $\mathcal{F}_h$ which is represented by

$$\underrightarrow{a}^{vs/h} = \underrightarrow{v}^{vs/h^{\bullet h}} = \frac{\underrightarrow{f}^{vg} + \underrightarrow{f}^{vt}}{m_v}. \tag{3.7}$$

where the off-nominal thrust resolved in $\mathcal{F}_h$ is

$$\underrightarrow{f}^{vt} = \underrightarrow{\boldsymbol{\mathcal{F}}}_h^{\mathsf{T}} \, \mathbf{C}_3(\delta_\theta) \, \bar{\mathbf{f}}_h^{vt}(1 + \delta_T), \tag{3.8}$$

$\bar{\mathbf{f}}_h^{vt}$ is the nominal force on the vehicle due to thrust resolved in $\mathcal{F}_h$, $\delta_T \sim \mathcal{N}(0, \sigma_T^2)$, and $\delta_\theta \sim \mathcal{N}(0, \sigma_\theta^2)$. The zero-mean normally distributed random variables slightly rotate the thrust force vector and change the thrust magnitude over time. The random parameters will be further discussed in Section 3.6 and the variances will be defined.

3.4 VEGA Measured Trajectory Equations of Motion

The truth model will be estimated by VEGA observations, incorporating additional measurement noise from VEGA. The VEGA measured equation of motion can be used to simulate dead reckoning, assuming that the spacecraft uses the measurements to correct the trajectory. The equation of motion can be defined as the acceleration of the vehicle relative to the sun with respect to $\mathcal{F}_h$ as measured by

VEGA, given by

$$\underset{\rightarrow}{a}^{vs/h} = \underset{\rightarrow}{v}^{vs/h^{\bullet h}} = \frac{\underset{\rightarrow}{f}_g^{\,v} + \underset{\rightarrow}{f}^{\,vt}}{m_v} + \underset{\rightarrow}{\delta}^{\,a}, \tag{3.9}$$

where VEGA acceleration noise measured in $\mathcal{F}_b$ is

$$\underset{\rightarrow}{\delta}^{\,a} = \underset{\rightarrow}{\boldsymbol{\mathcal{F}}}_b^{\mathsf{T}}\, \boldsymbol{\delta}_b^a \sim \mathcal{N}\left[\begin{pmatrix} 0 \\ 0 \\ 0 \end{pmatrix}, \begin{pmatrix} \sigma_a^2 \\ \sigma_a^2 \\ 0 \end{pmatrix}\right].$$

The zero-mean normally distributed random variable adds measurement in the body plane directions directions in the plane of the trajectory. No measurement noise is added in $\underset{\rightarrow}{b}^{\,3}$ since the analysis is performed in the plane defined by $\underset{\rightarrow}{b}^{\,1}$ and $\underset{\rightarrow}{b}^{\,2}$ which coincide with the ecliptic plane.

3.5 Observations

After solving the equations of motion for a given set of initial conditions and duration it is necessary to analyze the results as observations. These observations would take place on Earth through DSN tracking facilities and onboard the vehicle through VEGA acceleration measurements.

The simulation is completed in $\mathcal{F}_h$ and is required to be transformed to $\mathcal{F}_g$. The transformation is a clockwise rotation about $\underset{\rightarrow}{h}^2$ equal to 23.44^o, as discussed in Section 3.1. As a result, the position and velocity of the vehicle in $\mathcal{F}_g$ is

$$\mathbf{r}_g^{ve} = \mathbf{C}_2(-23.44^o)(\mathbf{r}_h^{vs} - \mathbf{r}_h^{es})$$

and

$$\mathbf{v}_g^{ve} = \mathbf{C}_2(-23.44^o)(\mathbf{v}_h^{vs} - \mathbf{v}_h^{es})$$

respectively. Here $\mathbf{r}_g^{ve}$ is the position of the vehicle relative to Earth resolved in $\mathcal{F}_g$, $\mathbf{r}_h^{vs}$ is the position of the vehicle relative to the Sun resolved in $\mathcal{F}_h$, and $\mathbf{r}_h^{es}$ is the position of the Earth relative to the Sun resolved in $\mathcal{F}_h$. Similarly, $\mathbf{v}_g^{ve}$ is the velocity of the vehicle relative to Earth resolved in $\mathcal{F}_g$.

Subsequently, one can calculate the required DSN observation data. The DSN range, range rate, right ascension, and declination are respectively given by

$$r = \left\|\mathbf{r}_g^{ve}\right\|, \tag{3.10}$$

$$rr = \mathbf{v}_g^{ve} \cdot \frac{\mathbf{r}_g^{ve}}{\left\|\mathbf{r}_g^{ve}\right\|}, \tag{3.11}$$

$$RA = \arctan(-r_{g1}^{ve}/r_{g2}^{ve}), \tag{3.12}$$

$$dec = \arctan\left(\frac{r_{g3}^{ve}}{\sqrt{r_{g1}^{ve^2} + _{g2}^{ve^2}}}\right), \tag{3.13}$$

where $\mathbf{r}_g^{ve} = [r_{g1}^{ve}\ r_{g2}^{ve}\ r_{g3}^{ve}]^\intercal$.

The second necessary transformation is the acceleration components of the spacecraft from $\mathcal{F}_h$ to $\mathcal{F}_b$, the spacecraft's body frame. The acceleration in the body frame will be used to simulate VEGA measurements. Since VEGA is an inertial measurement unit it will not measure acceleration due to gravity and this will be subtracted out of the total acceleration. The transformation is a rotation which is dependent on the spacecraft's position at a given time. The angle of rotation along $\underrightarrow{h}^3$ is

$$\theta = tan^{-1}(v_{g2}^{vb}/v_{g1}^{vb}),$$

where $\mathbf{v}_g^{ve} = [v_{g1}^{ve}\ v_{g2}^{ve}\ v_{g3}^{ve}]^\intercal$. The acceleration of the spacecraft in $\mathcal{F}_b$, as measured by VEGA, is

$$\mathbf{a}_g^{ve} = \mathbf{C}_3(\theta)(\mathbf{a}^{vb/h} - \mathbf{a}^{vb/h,g}). \tag{3.14}$$

where $\mathbf{a}^{vb/h}$ is the total acceleration acting on the spacecraft and $\mathbf{a}^{vb/h,g}$ is the acceleration acting on the spacecraft due to gravity.

3.6 Stochastic Modeling

There are several stochastic processes that occur during the mission that VEGA can be used to measure in real-time in order to facilitate dead reckoning. These uncertainties will be used to randomly generate several outcomes in a Monte Carlo simulation for analysis on VEGA's performance. The main stochastic processes that will affect the trajectory are random variations in the thrust magnitude, uncertainty in the thruster direction relative to the spacecraft, and noise in the VEGA's acceleration measurements. These were modeled as zero-mean normally distributed variables with standard deviations as shown in table 3–1.

Table 3–1: Modelled parameter uncertainties.

Parameter	σ
Thrust Magnitude	2% nominal
Thrust Direction	1 degree
VEGA acc. measurement	1 nG

Thrust magnitude and direction variations were based on the DS1 mission as described in [9]. VEGA's uncertainty model was based on the manufacturers specifications for the noise parameters such as the power spectral density shown in figure 3–4. The thrust magnitude variations are caused by power fluctuations and randomly occurring processes within the propulsion system. Additional attitude uncertainty can be described by as good as 3σ error of $1\mathrm{e}^{-}3$ degrees if required (J. L. Crassidis and R. Carpenter, personal communication, March 29, 2018), therefore it was decided these effects would be negligible compared to the thrust direction misalignment.

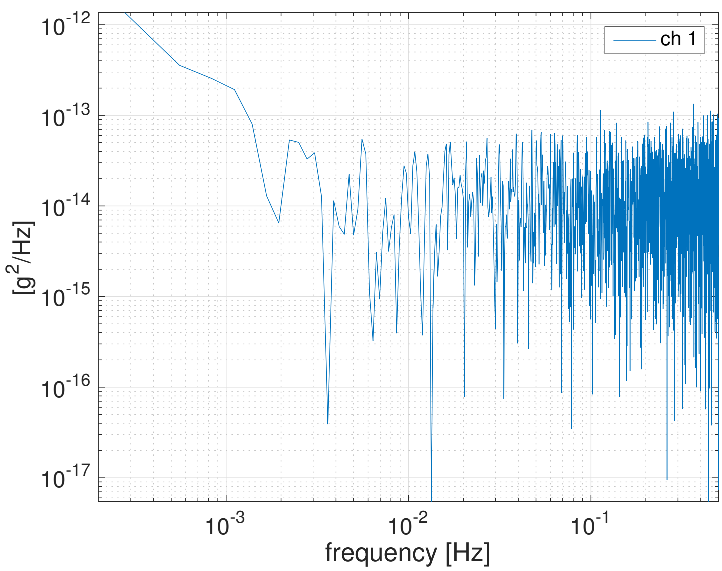

Figure 3–4: VEGA's noise power spectral density as specified by GEDEX Systems Inc.

In order to generate VEGA's noise characteristics, two noise signals were generated. One signal was normally distrusted white noise , as defined in table 3–1, and the second was an integrated white noise component. The effect of these combined noise signals is acceleration measurements which have random zero mean noise, but also exhibit transient variations known as a random walk. The generated noise of VEGA due to these effects is shown in figure 3–5.

In order to implement these variations a normally distributed random number generator was used in Matlab. The random number generator was seeded at each time step in order to ensure convergence. Several runs were produced in a Monte

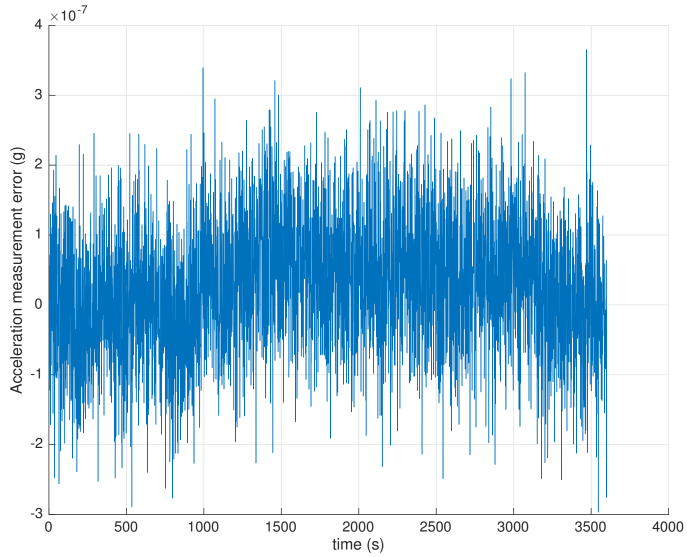

Figure 3–5: VEGA's measurement noise in one dimension.

Carlo analysis of possible outcomes to determine VEGA's dead-reckoning performance.

3.7 Interplanetary Trajectory Analysis

In order to asses the dead-reckoning accuracy and desired target-relative trajectory control for mission objectives the target-relative coordinate system, $\mathcal{F}_b$, is used. Since the position components expressed in $\underset{\rightarrow}{b}^1$ is orthogonal to the plane of the incoming asymptote of the spacecraft's approach trajectory, it can be used as a target miss parameter. The geometry of the B-Plane used for targeting is shown for a generalized case, where $\theta \neq 0$, in Figure 3–6. For the purpose of analyzing VEGA's performance a B-plane miss characteristic will be incorporated in the results for analysis.

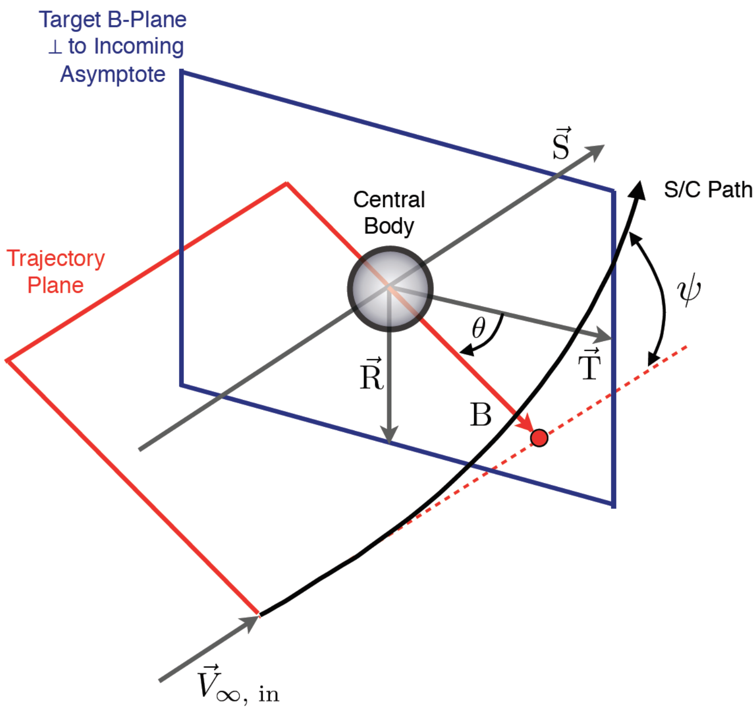

Figure 3–6: B-Plane targeting geometry. The B-Plane is orthogonal to the spacecraft's approach asymptote, and intersects the target body center [34].

CHAPTER 4
Model Validation Cases

In chapter 3, the mathematical model describing the dynamics of the system has been derived. This model will now be validated numerically to verify the equations the equations of motion are correct and the numerical implementation is sound.

4.1 Baseline Case

The nominal model of the system is simulated over a year in order to asses the behavior of the model. In Case 1 we will run the simulate with no thrust and observe the motion of the system. Since the system is only acting under two-body gravitational forces the spacecraft trajectory should remain circular. The trajectory for Case 1 is shown in figure 4–1.

As expected the trajectory remains circular around the Sun, matching the orbit of the Earth since this was the spacecraft's initial orbit. We can also numerically verify the results by checking the conservation of energy of the system. The gravitational potential, kinetic, and total energy are given by

$$U_g = -\frac{\mu_s m_v}{\|\mathbf{r}_h^{vs}\|}, \tag{4.1}$$

$$E_k = 0.5 m_v \left\|\mathbf{v}_h^{vs}\right\|^2, \tag{4.2}$$

$$E = U_g + E_k. \tag{4.3}$$

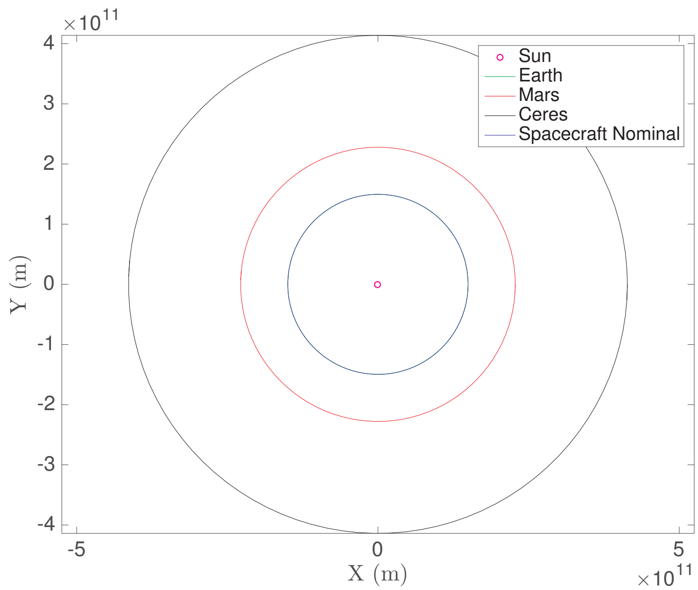

Figure 4–1: B-Plane targeting geometry.

Using equation 4.3 we can determine the change in the energy of the system over the simulation. The percent change in energy over the course of the simulation is shown in figure 4–2. Here the maximum percent change in energy is $1\text{x}10^{-13}\%$. For comparison the numerical absolute and relative tolerance were set to $1\text{x}10^{-15}$ and $1\text{x}10^{-14}$ respectively for this simulation. Therefore it is assumed that the change in energy is negligible and can be attributed to numerical roundoff.

4.2 Additional Cases

Three additional cases which incorporated constant thrust were also considered. Case 2 was given a thrust of 45 mN, half that of the nominal thrust. Case 3 was given a thrust of 90 mN, equal to that of the nominal thrust. Case 4 was given a thrust of 135 mN, equal to 1.5 times the nominal thrust. The total work done by thrust was calculated for these simulations and compared to the change in energy of the system

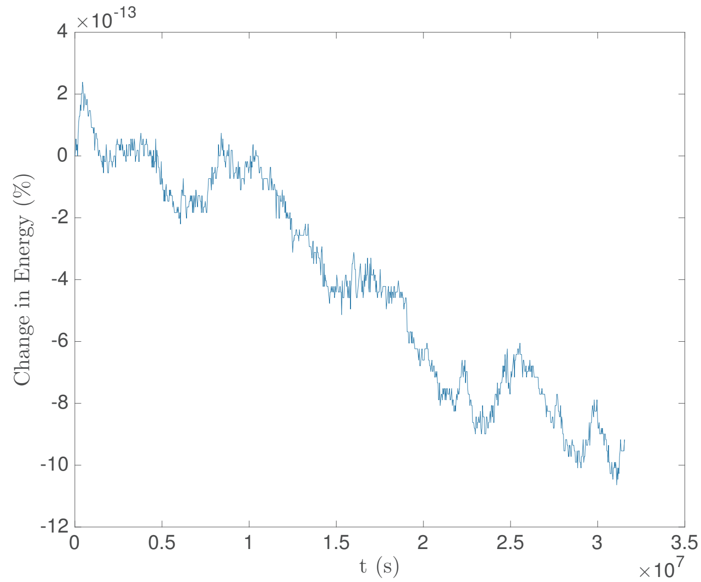

Figure 4–2: Case 1 change in energy over a year.

to assess. The inclusion of thrust increases the total energy of the system, however the difference between change in energy and work done by the thrust is still not very significant, on the order of 1x10^{-}5 over a year. These results are consistent with the conservation of energy, and therefore the dynamics model is valid. The results of the verification for all cases is summarized in table 4–1.

Table 4–1: Summary of model verification results

Case	1	2	3	4
Thrust (mN)	0	45	90	135
KE final (J)	3.33E+11	2.86E+11	2.42E+11	2.08E+11
U final (J)	-6.65E+11	-5.78E+11	-4.95E+11	-4.24E+11
E final (J)	-3.33E+11	-2.92E+11	-2.53E+11	-2.16E+11
ΔE (J)	0.003051758	4.10E+10	7.97E+10	1.17E+11
W (J)	0	4.10E+10	7.97E+10	1.17E+11
ΔE - W (J)	-9.17E-15	-4.61E-06	-1.88E-05	-3.99E-05

CHAPTER 5
Results and Discussion

This chapter presents results from a study of off-nominal effects on spacecraft trajectories, Monte Carlo simulations of VEGA's dead reckoning capabilities, and a mission impact assessment of the dead reckoning solution.

5.1 Study of Off-Nominal Effects

Before assessing VEGA's dead reckoning potential a preliminary study was done on the effects of various off-nominal effects that would be encountered in a mission. These effects included thrust magnitude random variations, thrust magnitude constant offset, thrust magnitude linear degradation over time, thrust direction constant off-pointing, and thrust direction linearly wandering over time. In addition, the impact of these effects were assessed based on the impact to the trajectory and DSN measured variable such as range, range-rate, right ascension, and declination.

The first case was the linear degradation of thrust over time. This was motivated by results seen in the Deep Space 1 mission where thrust degraded 3% from the nominal pre-launch value over the course of the mission. For this case the initial thrust was taken as 90mN and this was decreased by 5% over linearly over the duration of the mission. The actual thrust is

$$\underset{\rightarrow}{f}^{\,t} = (1 - 0.95t/t_f)\,\underset{\rightarrow}{\bar{f}}^{\,t} \tag{5.1}$$

where $\underset{\rightarrow}{f}^{\,t}$ is the nominal thrust, t is the elapsed time of the trajectory, and t_f is the final or total time of the trajectory.

The impact of these effects on the trajectory of spacecraft is shown in figure 5–1. In addition, the impact on the range, range rate, right ascension, and declination are shown in figure 5–2, 5–3, 5–4, and 5–5 respectively.

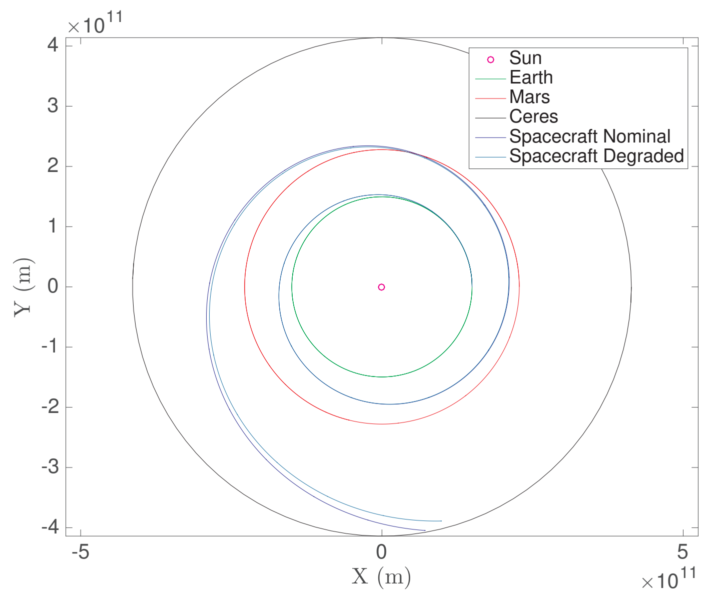

Figure 5–1: Trajectory due to thrust magnitude degradation of 5% over mission duration.

As expected the trajectory falls short of reaching the same radial distance as the nominal case due to the loss of thrust magnitude. The max error as would be measured by the DSN for range, range rate, right ascension, and declination was approximately 1 million km, 2000 m/s, 5 degrees, and 1.6 degrees. The DSN measured error is computed in order to asses the potential to lose track of the spacecraft due to large plane of sky error, as the combined effect of right ascension and declination error.

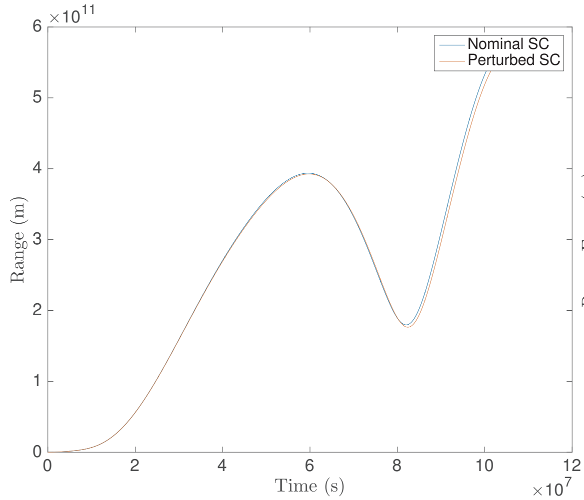

(a) Nominal and perturbed range curves.

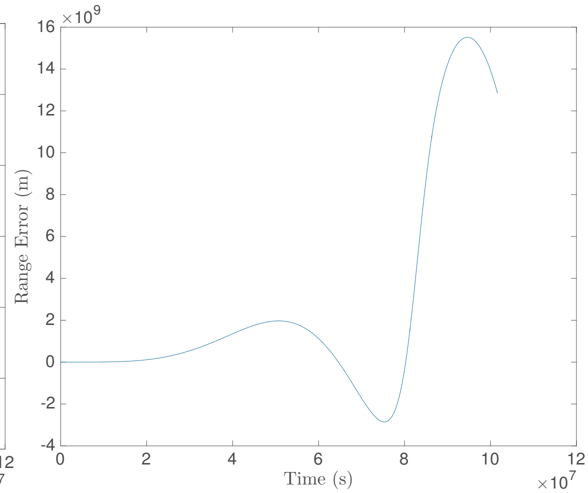

(b) Perturbed range error.

Figure 5–2: Range comparison for nominal and thrust magnitude degradation trajectories.

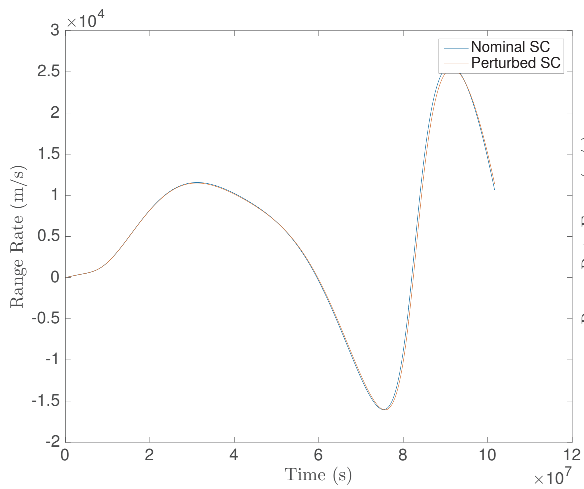

(a) Nominal and perturbed range rate curves.

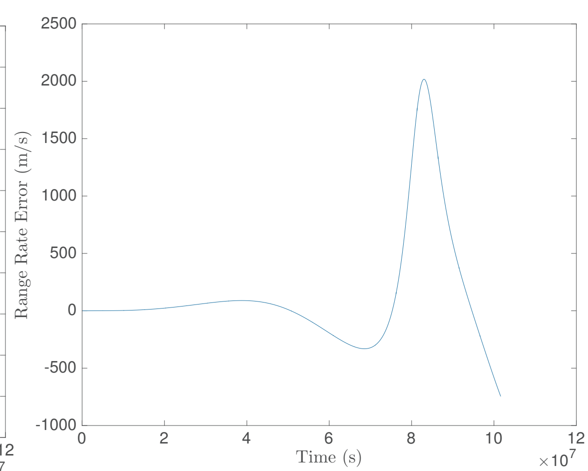

(b) Perturbed range rate error.

Figure 5–3: Range rate comparison for nominal and thrust magnitude degradation trajectories.

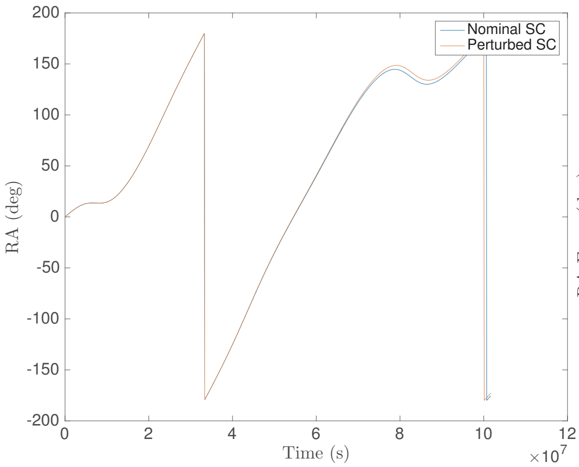

(a) Nominal and perturbed right ascension curves.

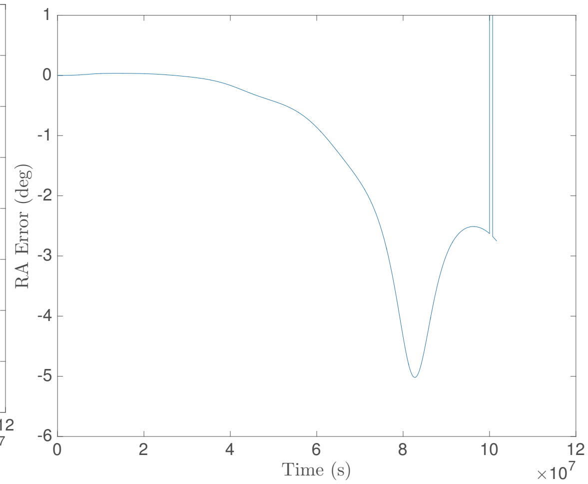

(b) Perturbed right ascension error.

Figure 5–4: Right ascension comparison for nominal and thrust magnitude degradation trajectories.

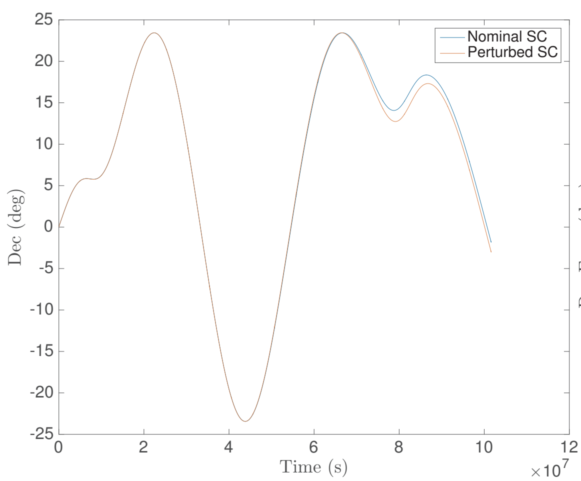

(a) Nominal and perturbed declination curves.

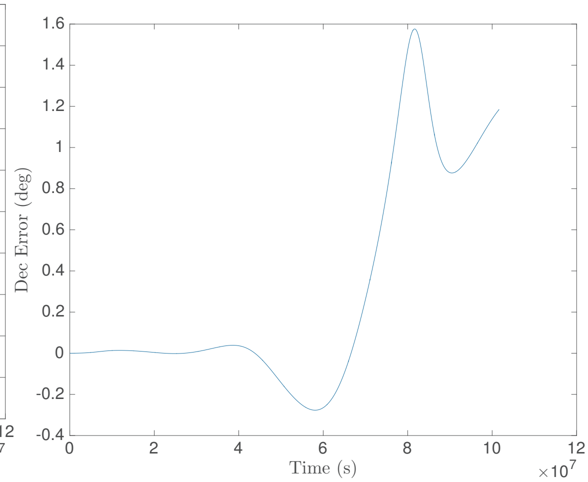

(b) Perturbed declination error.

Figure 5–5: Declination comparison for nominal and thrust magnitude degradation trajectories.

A simulation was also performed for random thrust magnitude variations over the duration of the mission. The thrust variation used was random variable within +/-5% of nominal thrust. The results on the trajectory is shown in figure 5–6.

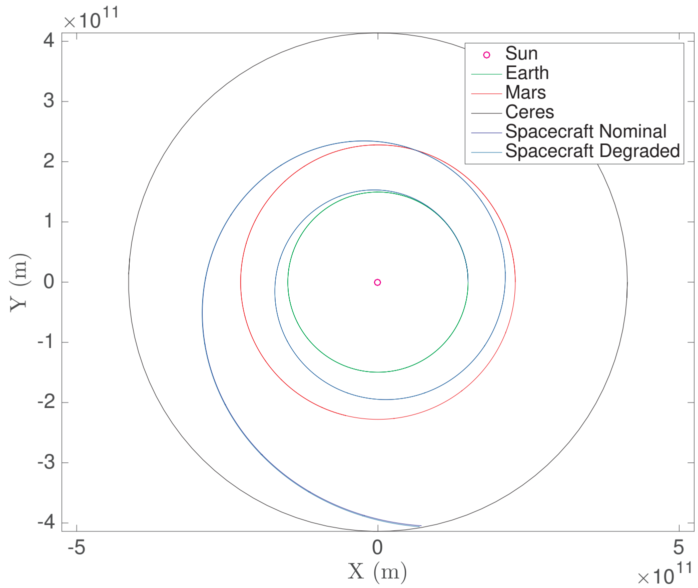

Figure 5–6: Trajectory due to random thrust fluctuations over mission duration.

An additional simulation was done to investigate the effect of constant thrust direction offset due to misalignment. The effect of a 10 degree misalignment in both directions is shown in figure 5–7. As expected a 10 degree misalignment has a very substantial effect on the trajectory, however this is significantly larger than would be expected in an actual mission.

Through these results it was realized that the largest impact on the trajectory would be from thrust magnitude effects. In addition, in this worst case scenario the plane of sky error is likely not to be higher then a few degrees as shown in the thrust magnitude degradation case. Therefore it would be unlikely to lose the spacecraft

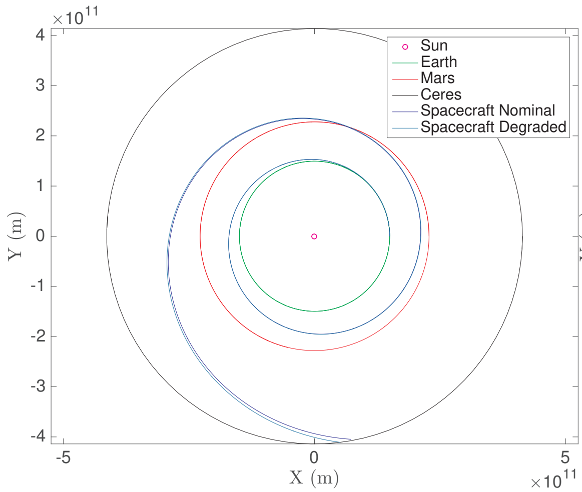

(a) Clockwise misalignment. **(b)** Clockwise misalignment.

Figure 5–7: Trajectory due to misalignment of thruster relative to spacecraft body.

due to plane of sky errors. In addition, the plane of sky error is highly dependent on the position of the Earth relative to the spacecraft which could be affected by several mission specific variables and might not be the best universal metric. Using this information it was decided to use b-plane targeting to assess the dead reckoning solution instead of plane of sky error.

5.2 Monte Carlo Results

In this section the dead reckoning solution is assessed through a Monte Carlo simulation of ten runs. The simulation uses the equations of motion and uncertainty characteristics discussion in Chapter 3. The duration of the simulation is three years, the approximate time required to reach the main asteroid belt. The trajectory overview of the simulation is shown in figure 5–8 and a close up view of final end state is shown in figure 5–9.

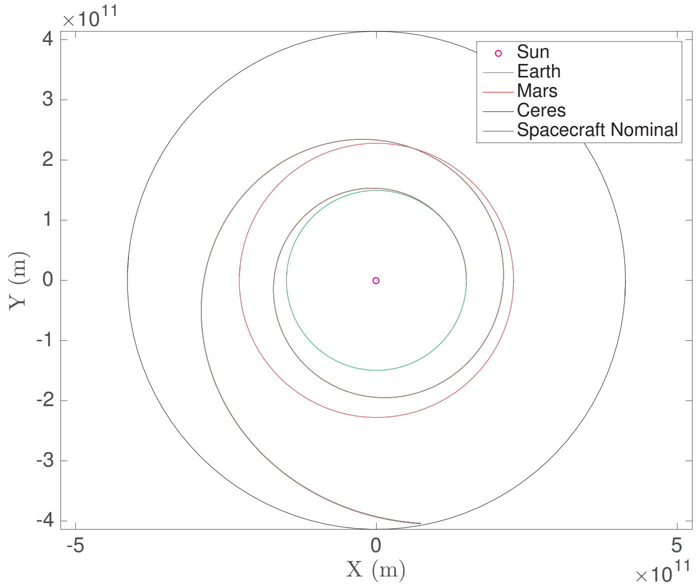

Figure 5–8: Overview of Monte Carlo dead reckoning trajectories.

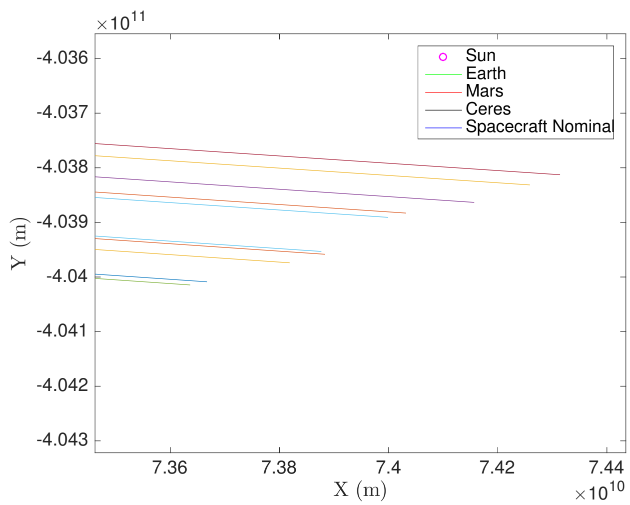

Figure 5–9: Close up view of Monte Carlo dead reckoning final trajectories.

It can be seen that there is significant dispersion among the different runs due to the random effects acting on the spacecraft. The trajectory overview contains both the actual trajectories and VEGA measured trajectories. In addition, it can be seen that the trajectories mostly fall in two close pairs, indicating that VEGA measured trajectories are closely trailing the actual trajectories.

Acceleration measurement error is defined as the different between the acceleration in the actual trajectory and the VEGA measured trajectory. Acceleration measurements can be divided into two components, gravitational and non-gravitational. It can also be separated into two direction components, the velocity tangential and radial component. Non-gravitational acceleration measurement error in the radial and tangential directions are shown in figure 5–10. This is also effectively VEGA's measurement error since there is no other non-gravitational disturbance in the acceleration.

Gravitational acceleration error in the radial and tangential directions are shown in figure 5–11. It is shown that the gravitational acceleration error is initially zero since all cases start at the same position and gravitational acceleration is dependent on heliocentric distance. However, as the position of the spacecraft change due to non-gravitational measurement errors this causes gravitational acceleration to change which further perturbs the motion.

Total acceleration error in the radial and tangential directions are shown in figure 5–12. Very early on in the trajectory non-gravitational measurement errors dominate due to VEGA, however for the majority of the time the dominant effects mostly are due to gravitational forces. This can be seen in the close similarity of the gravitational acceleration error and total acceleration error curves.

The position measurement error in the radial and tangential directions are shown in figure 5–13a and figure 5–13b respectively.

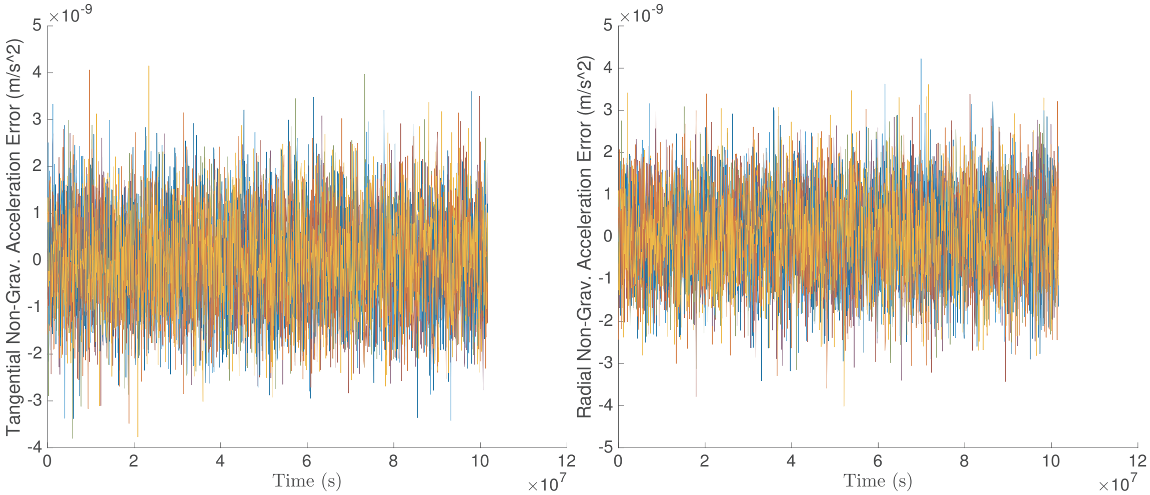

(a) Tangential direction. **(b)** Radial direction.

Figure 5–10: Non-gravitational acceleration error.

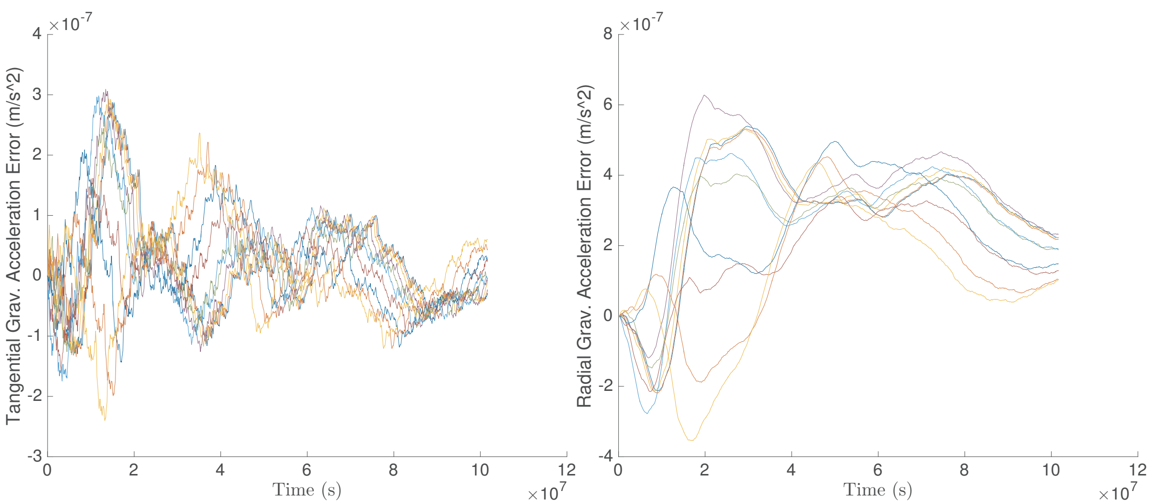

(a) Tangential direction. **(b)** Radial direction.

Figure 5–11: Gravitational acceleration error.

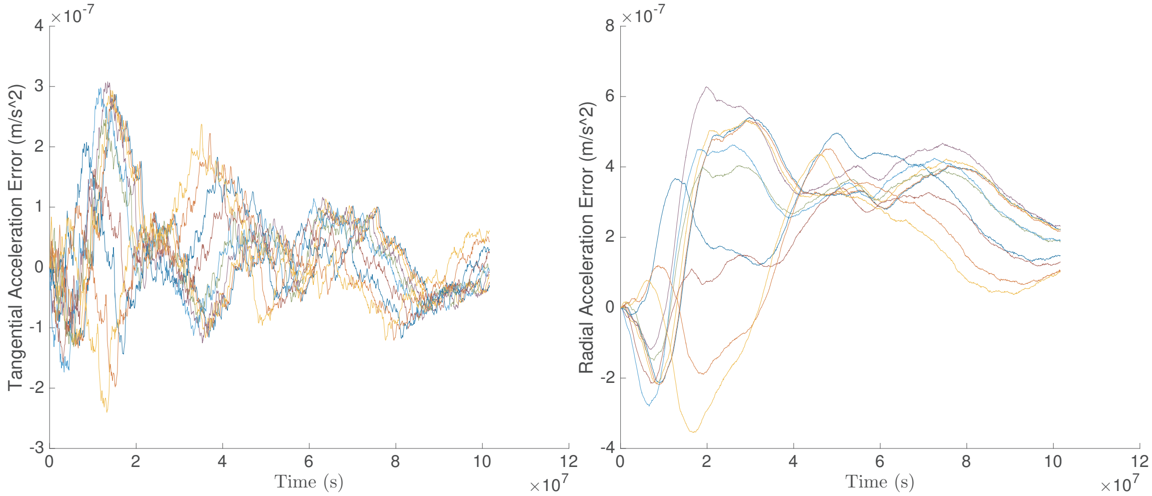

(a) Tangential direction. **(b)** Radial direction.

Figure 5–12: Total acceleration error.

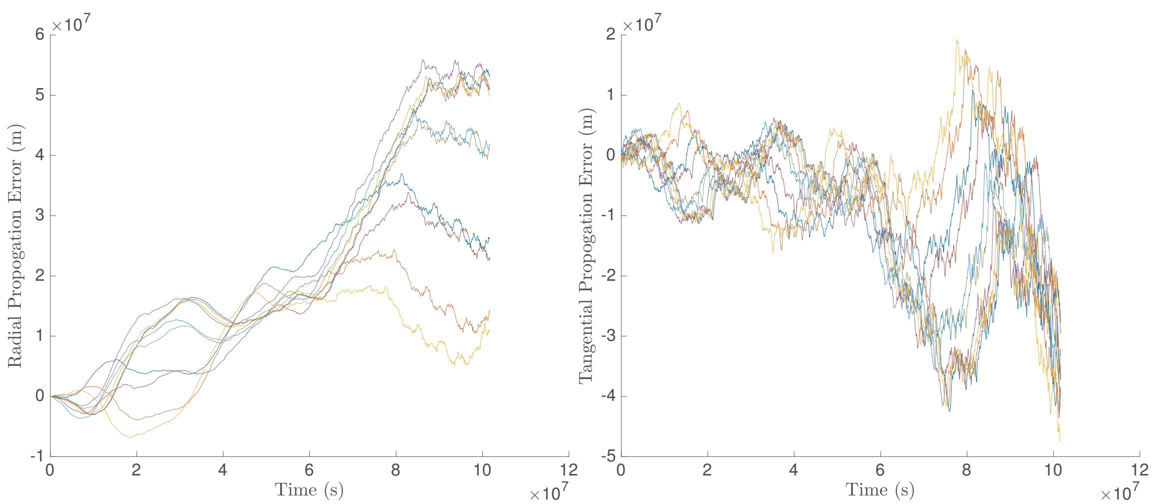

(a) **(b)**

Figure 5–13: Total dead reckoning position error.

The position error corresponds directly to the double integration of the acceleration error, which the dead reckoning solution would be based upon. Final B-plane propagation miss error is defined as position measurement error between VEGA and actual position, in the radial direction. As previously discussed, this will be used as the basis to determine the effectiveness of the dead reckoning solution. Nominal error is defined as the difference between the acceleration of the nominal trajectory and the actual trajectory. VEGA error is defined as the difference between the acceleration of the VEGA measured trajectory and the actual trajectory. These can be compared to asses the difference between current error before tracking to VEGA error for a similar period.

The nominal B-plane propagation error after 7 days is shown in figure 5–14. The VEEGA B-plane propagation error after 7 days is shown in figure 5–15.

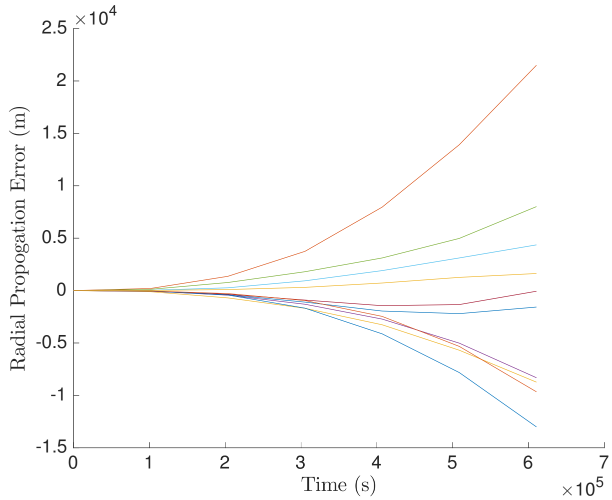

Figure 5–14: Nominal targeting error after 7 days.

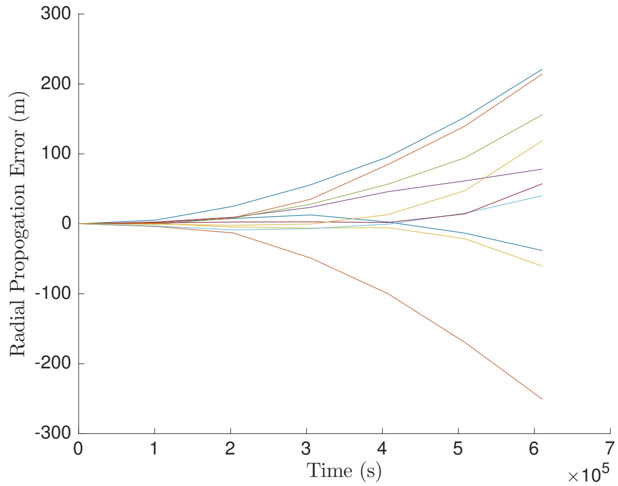

Figure 5–15: VEGA targeting error after 7 days.

Similarly, VEGA B-plane propagation error after 30 days is shown in figure 5–16.

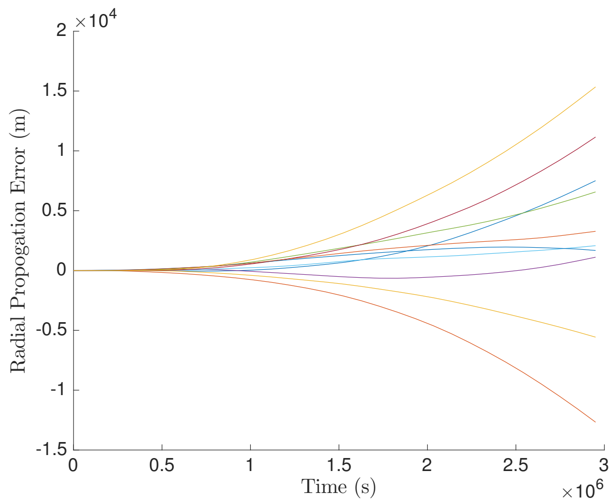

Figure 5–16: VEGA targeting error after 30 days.

Comparing VEGA B-plane targeting position error and nominal plane targeting position we can asses how much better VEGA can detect changes in trajectory to perform dead reckoning. From figure 5–14 it can be shown that after 7 days the spacecraft is approximately 10 km off it's target at worst. From figure 5–16 it can be shown that it takes 30 days for VEGA measurements to produce the same level of error. Therefore, this means that using VEGA for dead reckoning would allow the spacecraft to use deep space tracking facilities 3 times less, from once a week to once a month.

5.3 VEGA Mission Application Impact

Based on the results in Section 5.2 we can now assess the impact of VEGA dead reckoning on mission capabilities. As typical low-thrust interplanetary mission will have weekly thrusting sessions which must be broken up by a coasting period with a tracking session as shown in figure 5–17. This is done to align the spacecraft antenna which is typically in an unfavorable attitude for thrusting. Tracking is done in order to verify the position of the spacecraft since a certain amount of position uncertainty has accrued since last tracking sessions. However, VEGA dead reckoning can be used to extend the thrusting period and delay radio tracking sessions.

As discussed in [8], DSN tracking sessions cost approximately 10,000 USD per session. Therefore, if VEGA required radiometric tracking three times less per month over the course of a three-year mission, in total that will amount to 108 less tracking sessions over the course of the mission. This corresponds to mission savings over one mission USD. Alternatively, this would also allow a mission extension of three times as long for the same radiometric tracking budget.

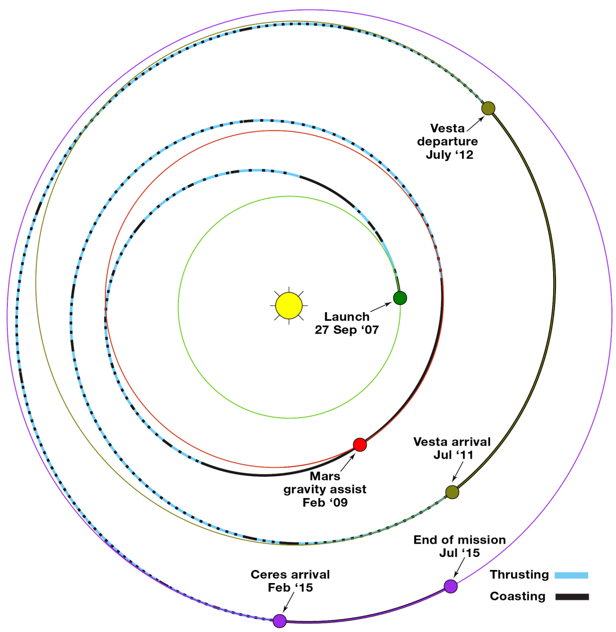

Figure 5–17: Typical low-thrust interplanetary trajectory with thrusting and coasting phases shown.

CHAPTER 6
Conclusions and Future Work

Low-thrust navigation has several advantages for deep space missions but suffers from significant performance variations that can impact a mission. There has also been advances in accelerometer technology, such as that used by VEGA. While in the past low-thrust inertial navigation has not been possible due to relatively large errors in measurements, these advances show promise for enabling inertial navigation. This work has been motivated by the need to investigate the efficacy of VEGA dead reckoning for low-thrust interplanetary navigation.

The effectiveness of VEGA was shown by simulating its performance in a low-thrust mission. First, a low-thrust trajectory simulation was created. Next, several perturbing effects due to uncertainty in thrust were added along with VEGA acceleration noise. Using this model a Monte Carlo simulation was created to investigate the dead-reckoning position errors. It was shown that the targeting position error of VEGA after 30 days is comparable to nominal errors after 7 days. This would enable three times less tracking sessions per month, allowing for significant cost savings over the mission.

Considering the increasing number of interplanetary missions similar to this study, the benefits of VEGA dead reckoning would allow added mission capabilities and help reduce reliance on the DSN. This also shows potential for enabling increased commercial activity in deep space.

Future work is needed to further asses the ability of dead reckoning in mission. In order to so, a Kalman filter framework should be developed to predict and correct the dead reckoning solution in real time. This will be a better indication of real mission performance. In addition, while this study was carried out in solely in the ecliptic plane, out of plane effects should also be investigated.

REFERENCES

[1] B. Dunbar, "Deep Space Network,"NASA, 24-Apr-2015. [Online]. Available: http://www.nasa.gov/directorates/heo/scan/services/networks/dsn. [Accessed: 16-Apr-2018].

[2] N. A. Renzetti, "DSN Functions and Facilities."

[3] J. Taylor, "Deep Space Communications," NASA Jet Propulsion Lab. [Online]. Available: https://descanso.jpl.nasa.gov/monograph/series13_chapter.html. [Accessed: 16-Apr-2018].

[4] L. J. Wood, "Guidance, Navigation, and Control Technology Assessment ...," NASA Solar System Exploration. [Online]. Available: https://solarsystem.nasa.gov/resources/289/guidance-navigation-and-control-technology-assessment-onboard-and-ground-navigation-and-mission-des/?category=reports. [Accessed: 16-Apr-2018].

[5] E. Y. Choueiri, "New Dawn for Electric Rockets," Scientific American, vol. 300, no. 2, pp. 5865, 2009.

[6] M. B. Quadrelli, L. J. Wood, J. E. Riedel, M. C. Mchenry, M. Aung, L. A. Cangahuala, R. A. Volpe, P. M. Beauchamp, and J. A. Cutts, "Guidance, Navigation, and Control Technology Assessment for Future Planetary Science Missions," Journal of Guidance, Control, and Dynamics, vol. 38, no. 7, pp. 11651186, 2015.

[7] "NASA Space Technology Roadmaps and Priorities," National Research Council of the National Acadamies, Jul. 2012.

[8] "NASAs Mission Operations and Communications Services," NASA Jet Propulsion Lab. [Online]. Available: https://deepspace.jpl.nasa.gov/files/NASA_MO&CS.pdf. [Accessed: 16-Apr-2018].

[9] B. Kennedy, "DESCANSO Design and Performance Summary Series - NASA." [Online]. Available: https://descanso.jpl.nasa.gov/DPSummary/DS1_Navigation_Primary.pdf. [Accessed: 16-Apr-2018].

[10] "Guidance, Navigation, and Control Technology Assessment Part II" [Online]. Available: https://solarsystem.nasa.gov/system/downloadable_items/155_GNC_Tech_Assess_Part_II_Onboar [Accessed: 16-Apr-2018].

[11] C. E. Kohlhase, "Autonomous Navigation Preparations for Future Unmanned Space Missions*," Navigation, vol. 22, no. 1, pp. 1634, 1975.

[12] D. A. Vallado and W. D. McClain,Fundamentals of astrodynamics and applications. Hawthorne, CA: Published by Microcosm Press, 2013.

[13] R. R. Bate, D. D. Mueller, and J. E. White,Fundamentals of astrodynamics. New York: Dover Publications, 2015.

[14] A. E. Bryson and Y.-C. Ho,Applied optimal control. Wash., D.C., 1975.

[15] 2014 Longuski J. M. LONGUSKI,OPTIMAL CONTROL WITH AEROSPACE APPLICATIONS. S.l.: SPRINGER-VERLAG NEW YORK, 2016.

[16] P. Venkataraman, Applied optimization with MATLAB programming. Hoboken, NJ: John Wiley & Sons, 2009.

[17] G. Genta and P. Maffione, "Optimal low-thrust trajectories for nuclear and solar electric propulsion," Acta Astronautica, vol. 118, pp. 251261, 2016.

[18] "Factorization methods for discrete sequential estimation G.J. Bierman Academic Press, New York, 1977, 241 pages.," Mathematics and Computers in Simulation, vol. 24, no. 6, p. 55, 1982.

[19] S. Bhaskaran, "Autonomous Navigation for Deep Space Missions," SpaceOps 2012 Conference, Nov. 2012.

[20] C. L. Thornton and J. S. Border, "Radiometric Tracking Techniques for Deep Space Navigation," 2003.

[21] A. Gipsman, M. Guelman, and A. Kogan, "Autonomous navigation and guidance system for low thrust driven deep space missions," Acta Astronautica, vol. 44, no. 7-12, pp. 353-364, 1999.

[22] L. J. Wood, "The Evolution of Deep Space Navigation: 1962-1989 - NASA." [Online]. Available: https://descanso.jpl.nasa.gov/evolution/AAS_08-051.pdf. [Accessed: 16-Apr-2018].

[23] W. G. Melbourne, "Navigation between the Planets," Scientific American, vol. 234, no. 6, pp. 5874, 1976.

[24] L. J. Wood, "THE EVOLUTION OF DEEP SPACE NAVIGATION: 1999-2004." [Online]. Available: https://descanso.jpl.nasa.gov/evolution/AAS_14-255.pdf. [Accessed: 16-Apr-2018].

[25] L. J. Wood, "THE EVOLUTION OF DEEP SPACE NAVIGATION: 2004-2006." [Online]. Available: https://descanso.jpl.nasa.gov/evolution/AAS_17-325.pdf. [Accessed: 16-Apr-2018].

[26] M. D. Rayman, T. C. Fraschetti, C. A. Raymond, and C. T. Russell, "Dawn: A mission in development for exploration of main belt asteroids Vesta and Ceres," Acta Astronautica, vol. 58, no. 11, pp. 605616, 2006.

[27] Y. Kobayashi, T. Ito, M. Mita, H. Takeuchi, R. Funase, A. Tomiki, D. Kobayashi, T. Nonomura, Y. Fukushima, and Y. Kawakatsu, "Low-cost and ultimately-downsized X-band deep-space telecommunication system for PROCYON mission," 2016 IEEE Aerospace Conference, 2016.

[28] P. Y. Peterson, H. Kamhawi, W. Huang, G. Williams, J. H. Gilland, J. Yim, R. R. Hofer, and D. A. Herman, "NASAs HERMeS Hall Thruster Electrical Configuration Characterization," 52nd AIAA/SAE/ASEE Joint Propulsion Conference, 2016.

[29] Border, J. S., Lanyi, G. E., and Shin, D. K., "Radio Metric Tracking for Deep Space Navigation," in Advances in the Astronautical Sciences: Guidance and Control 2008, Vol. 131, edited by M. E. Drews and R. D. Culp, Univelt, San Diego, 2008, pp. 309328.

[30] D. Doody, "Deep Space Craft," 2009.

[31] R. Cowen, "NASA Loses Mars Climate Orbiter," Science News, vol. 156, no. 14, p. 214, Feb. 1999.

[32] W. Wrigley, "History of Inertial Navigation," Navigation, vol. 24, no. 1, pp. 16, 1977.

[33] O. J. Woodman, "An introduction to inertial navigation," University of Cabridge Computer Laboratory, Aug. 2007.

[34] "THREE-DIMENSIONAL GRAVITATIONAL SWING-BYS BPlane Targeting." [Online]. Available: ccar.colorado.edu/imd/2015/documents/BPlaneHandout.pdf. [Accessed: 16-Apr-2018].